Technical Report Documentation Page

1. Report No.	2. Government Accession No.	3. Recipient's Catalog No.
FHWA/VA-93-R12		

4. Title and Subtitle	5. Report Date
Field Instrumentation and Measured Response of the I-295 Cable-Stayed Bridge: Part 1—Field Study of Live Load Responses	December 1992
	6. Performing Organization Code
7. Author(s) Paul S. Duemmel, Thomas T. Baber, Furman W. Barton, Wallace T. McKeel, Jr.	8. Performing Organization Report No. VTRC 93-R12
9. Performing Organization Name and Address Virginia Transportation Research Council Box 3817, University Station Charlottesville, Virginia 22903-0817	10. Work Unit No. (TRAIS) HPR Research Study No. 68
	11. Contract or Grant No.
12. Sponsoring Agency Name and Address Virginia Department of Transportation 1401 E. Broad Street Richmond, Virginia 23219	13. Type of Report and Period Covered Final Report – Part A
	14. Sponsoring Agency Code

15. Supplementary Notes

None

16. Abstract

This report describes the results of a field study of the live load responses of a segmentally constructed prestressed concrete cable-stayed bridge. The main span of the test structure consists of twin box girders connected by delta frames.

Known vehicular loadings were placed statically at various points along the bridge. Strains measured during this loading were compared with those obtained from finite element models of the bridge. Strain trends predicted by the finite element model were in good agreement with the measured strain trends. Quantitative agreement was fair, at least in part because of the high stiffness of the bridge and the limitations on the magnitude of load that could be applied.

17. Key Words	18. Distribution Statement
Load tests, prestressed concrete, cable-stayed bridges, field testing.	No restriction. This document is available to the public through the National Technical Information Service, Springfield, VA 22161.

19. Security Clasif. (of this report)	20. Security Classif. (of this page)	21. No. of Pages	22. Price
Unclassified	Unclassified	52	

FINAL REPORT

FIELD INSTRUMENTATION AND MEASURED RESPONSE OF THE I-295 CABLE-STAYED BRIDGE: PART 1—FIELD STUDY OF LIVE LOAD RESPONSES

Paul S. Duemmel
Graduate Research Assistant

Thomas T. Baber
Faculty Research Scientist

Furman W. Barton
Faculty Research Scientist

Wallace T. McKeel, Jr.
Research Manager

Virginia Transportation Research Council
(A Cooperative Organization Sponsored Jointly by the Virginia Department of Transportation and the University of Virginia)

In Cooperation with the U.S. Department of Transportation
Federal Highway Administration

Charlottesville, Virginia

December 1992
VTRC 93-R12

928

BRIDGE RESEARCH ADVISORY COMMITTEE

C. A. NASH, Chairman, Suffolk District Administrator, VDOT

W. T. MCKEEL, Executive Secretary, Senior Research Scientist, VTRC

G. W. BOYKIN, Suffolk District Materials Engineer, VDOT

N. W. DILLON, Salem District Structures & Bridge Engineer, VDOT

M. T. KERLEY, Salem District Structures and Bridge Engineer, VDOT

T. F. LESTER, Structures and Bridge Division, VDOT

L. L. MISENHEIMER, Staunton District Bridge Engineer, VDOT

C. NAPIER, Structural Engineer, Federal Highway Administration

W. L. SELLARS, Lynchburg District Bridge Engineer, VDOT

D. B. SPRINKEL, Culpeper District Structures and Bridge Engineer, VDOT

J. F. J. VOLGYI, JR., Structures and Bridge Division, VDOT

L. R. L. WANG, Professor of Civil Engineering, Old Dominion University

R. E. WEYERS, Professor of Civil Engineering, VPI & SU

ABSTRACT

This report describes the results of a field study of the live load responses of a segmentally constructed prestressed concrete cable-stayed bridge. The main span of the test structure consists of twin box girders connected by delta frames.

Known vehicular loadings were placed statically at various points along the bridge. Strains measured during this loading were compared with those obtained from a finite element model of the bridge. Strain trends predicted by the finite element model were in good agreement with the measured strain trends. Quantitative agreement was fair, at least in part because of the high stiffness of the bridge and the limitations on the magnitude of load that could be applied.

FINAL REPORT

FIELD INSTRUMENTATION AND MEASURED RESPONSE OF THE I-295 CABLE-STAYED BRIDGE: PART 1—FIELD STUDY OF LIVE LOAD RESPONSES

Paul S. Duemmel
Graduate Research Assistant

Thomas T. Baber
Faculty Research Scientist

Furman W. Barton
Faculty Research Scientist

Wallace T. McKeel, Jr.
Research Manager

INTRODUCTION

Cable-Stayed Bridges

Two relatively recent developments in bridge technology, segmentally erected, prestressed, concrete box girders and a cable-stayed support system, were employed on the James River Bridge near Richmond, Virginia. These innovations result in speedy erection and efficient use of high-strength materials, as well as pleasing aesthetics.

Until the early 1970s, concrete was not used in cable-stayed bridges because of its relatively low strength-to-weight ratio and the complexities of design; recent design simplifications and innovative construction techniques helped make it more competitive (Muller & McCallister, 1988). Segmental construction, by means of the cantilever method, is ideally suited to the stay cable support system (Mathivat, 1983). The cable-stayed segmental bridge scheme provides a number of benefits in addition to the obvious economic advantages. Concrete superstructures are well suited to stay cable configurations because the horizontal component of cable-stay forces produces prestressing in the deck. Concrete bridges also have favorable vibration damping characteristics, and their small live load–to–dead load ratio limits live load deflections. Today, cable-stayed segmental bridges are competitive for intermediate spans that had previously been constructed using variable-depth box girder designs. The James River Bridge, with a main span of 630 ft, is in this span range.

Cable-stayed, segmentally erected, prestressed bridges are challenging to analyze and design. The typical arrangement of several continuous spans with multiple supporting cables makes these structures highly statically indeterminate. Additional complexity is added by multistage post-tensioning, stay cable nonlinearity, connections, and variations of residual stress within the structure. Time-dependent deflections caused by creep and shrinkage of concrete and relaxation of stay cables and post-tensioning strands must also be considered. Finally, responses must be determined for complicated systems of mechanical and thermal loads.

The complex behavior of segmental post-tensioned bridges, coupled with the recent development of this technology, has led to significant problems. Severe cracking has seriously affected the serviceability of a number of bridges in the United States and Europe. This has generally been attributed to underestimation of stresses in design, along with improper construction techniques and inferior workmanship (Podolny, 1985). Such mechanisms alone usually produce only minor stresses, but together, the superposition of stresses can be high enough to cause cracking. Box girders with sloping webs have exhibited longitudinal flange cracking, induced by previously neglected transverse forces in inclined prestressing tendons (Podolny, 1986).

Numerous methods for analyzing segmental prestressed and cable-stayed bridges have been developed. Although these computational methods can easily provide response information, the information is meaningful only if it models the actual behavior of the bridge. Localized effects, such as those that occur at the connections between the stay cables and the bridge deck, cannot generally be ascertained feasibly with existing models. Field testing of complex bridge designs is therefore essential to validate computer models and gain insight into the actual behavior of bridges built using new and innovative structural technology.

Bridge field testing serves to provide localized response information unavailable from even complex analytical models and can aid in the development of reliable computer models for complex structures. Field studies have been conducted on a number of segmental prestressed bridges, and investigations of cable-stayed and segmental cable-stayed bridges are currently underway (Floyd & Sutton, 1982; Nam Shiu, 1985; Nam Shiu et al., 1983; Russell et al., 1982; Waldron et al., 1990). A research team from the University of Virginia (UVa) and the Virginia Transportation Research Council (VTRC) conducted the current live load field study of a segmental, cable-stayed, box girder bridge. A companion report describes a study of thermal stresses carried out concurrently (Duemmel et al., 1992).

Field tests of full-size structures may be carried out using either ambient or artificial loading conditions. Artificial loads have the advantage that their magnitudes can be determined more precisely, and they can be positioned more carefully than ambient loads. Hence, load testing of bridges in the field using artificial loading conditions is one effective means of studying actual bridge behavior. This is the method used in the studies reported herein.

The I-295 James River Bridge

The structure under investigation is a segmentally erected, precast, post-tensioned, cable-stayed box girder bridge that carries Interstate 295 over the James River approximately 15 miles southeast of Richmond, Virginia. The bridge has 28 individual spans, including approach spans. The focus of this study was a 7-span continuous section, which includes the 630-ft main (river crossing) span and three 150-ft approach spans at each end. The main span and the two adjacent spans on each side of the river are supported by a system of 52 cable stays arranged in a single plane harp configuration. The stays emanate from a pair of 290-ft pylons located on either side of the river. An elevation drawing of the bridge is shown in Figure 1.

The bridge deck is composed of two parallel box girders joined by a closure pour along the center line of the structure. The forces from the cable stays are transferred to the twin box girders through a series of precast delta frame assemblies located between the girders at each stay location, as shown in Figure 2. The main span of the bridge was constructed by the cantilever method, with two sides built outward from each pylon and connected by a closure pour at midspan. The segments are joined together by epoxy cement and post-tensioning strands within the flanges of the girders. The box girders are externally post-tensioned by a system of multiple tendons anchored within the deck segments. Figure 3 shows the cross-sectional dimensions of the main span segments, which are 10 ft long and weigh approximately 70 tons each. The bridge superstructure is supported on precast, segmental piers, along with the pylons, which are cast in place below deck level and are precast and segmental above. Figure 4 shows the twin box girders at the main pier/pylon locations.

The James River Bridge was completed in April 1990 and was opened to traffic in July 1990. It was the first cable-stayed bridge in Virginia and the first to employ the twin parallel box girder deck supported by a single plane of cable stays. This innovative scheme required less material than a single box girder of the same width, and the need for special construction equipment was significantly reduced (Muller & McCallister, 1988).

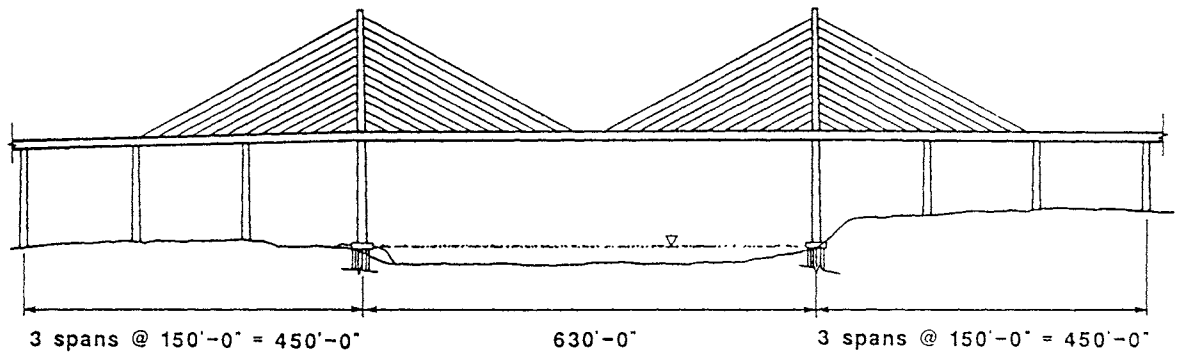

Figure 1. Central Spans of the I-295 Bridge.

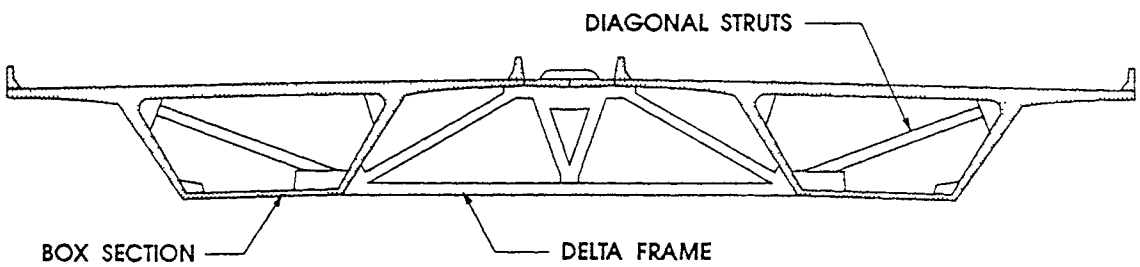

Figure 2. Cross Section of Twin Box Girder Showing a Typical Delta Frame.

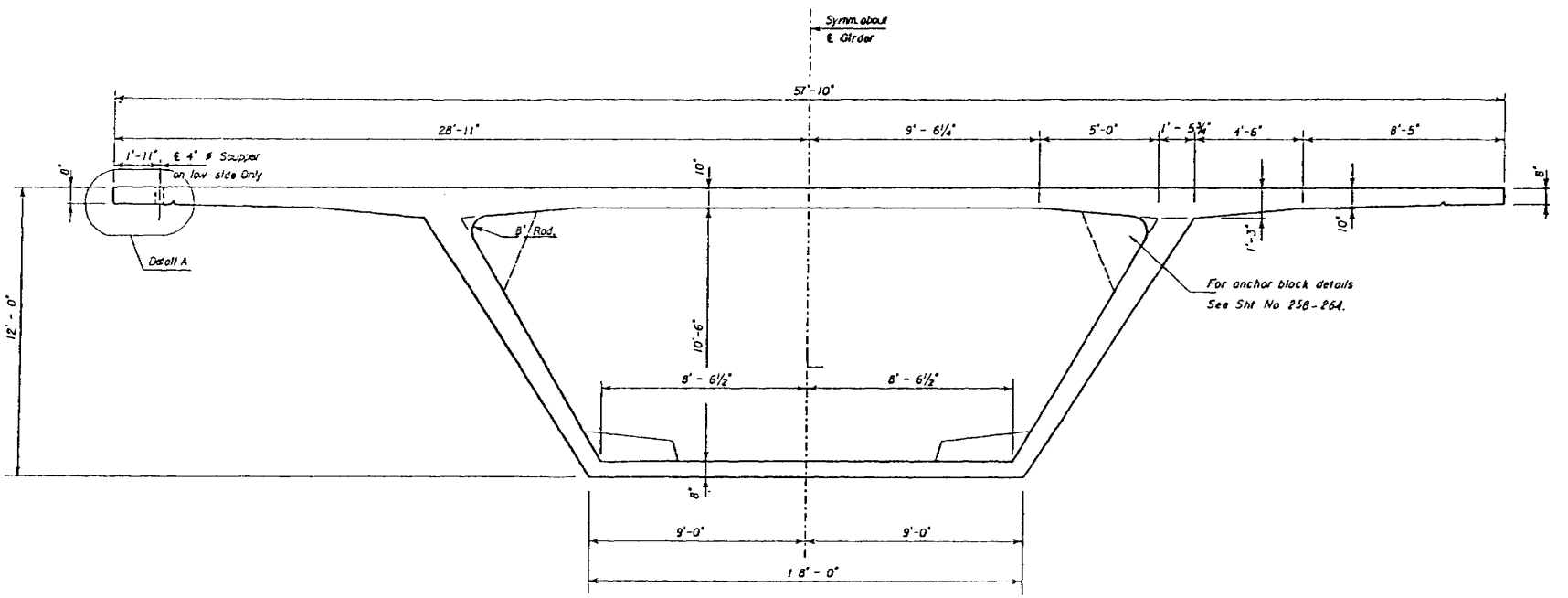

Figure 3. Dimensions of the Box Girder Cross Section.

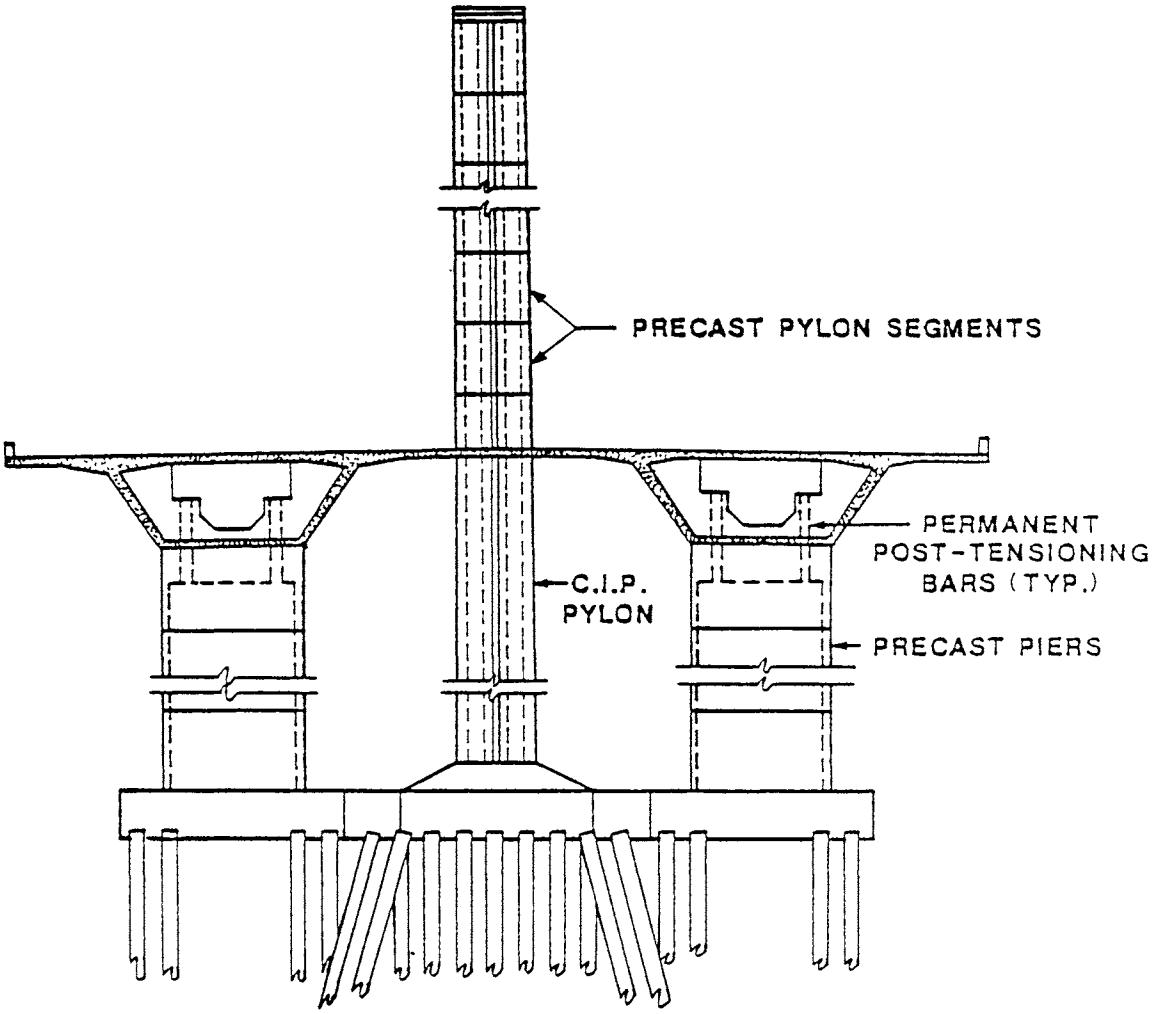

Figure 4. Bridge Section at Main Pier/Pylon Locations. CIP = cast in place.

PURPOSE AND SCOPE

The objective of the continuing UVa/VTRC study was to determine the important stresses of the James River Bridge during construction and then in service by the measurement of field responses. Previous work included measurement of strains in the box girders and cable stays during construction (Barton et al., 1991; Mohr, 1989). The present research had two objectives: measurement and evaluation of the response of the bridge under vehicle loads.

To meet these objectives, three tasks were undertaken:

1. A literature review was conducted to determine the expected types of deformation in a cable-stayed box girder bridge and the methods available for mechanical analyses of box girder bridges.

2. A heavily loaded truck was placed at various locations along the bridge, and strain measurements were taken using an array of strain gages located in three of the main-span box girder segments.

3. A detailed finite element model of the bridge was developed, and the data from this model were compared with the measured data.

LITERATURE REVIEW

Deformational Modes of Box Girder Bridges

The response of box girder sections to deformation may be quite complex. Maisel and Roll (1974) discussed the various modes of structural behavior of single box girders, and Baber and Hilton (1988) outlined the expected deformation modes of more complex twin box girder sections. The following paragraphs summarize the predominant deformation modes of the main-span box girders under applied mechanical loading.

The gross bending and torsional response of the twin box girder is expected to be similar to that of a less complex single box girder. The torsional behavior will, however, have two components: twisting of the two girders as a unit, caused by unbalanced external loads, and twisting of the girders relative to each other, resulting from cable-stay forces. Figure 5 illustrates the gross cross-sectional flexural and torsional behavior of the twin box girders. Assuming the cross section does not deform, all points will undergo identical vertical displacements in pure bending, as shown in Figure 5(a). This is the primary load-carrying mechanism expected. The unit twist of the two box sections about the plane of the cable stays attributable to unbalanced loading is depicted in Figure 5(b). Here, the delta frame assemblies eliminate independent rotation of the box girders. Figure 5(c) shows the relative torsional displacement between the two boxes that may occur as a result of the stay cable forces acting between the two girders. In this case, the delta frames, essentially concrete trusses between the box girders, are not infinitely stiff and do allow some relative twisting to occur. In reality, some degree of each of these deformation modes can be expected to occur simultaneously.

In addition to overall bending and torsional response, local deformations are expected in the box girder sections. The two types of local structural behavior that predominate are distortion and warping of the cross section. Distortion arises from transverse bending of the box girder walls, and three such modes are illustrated for

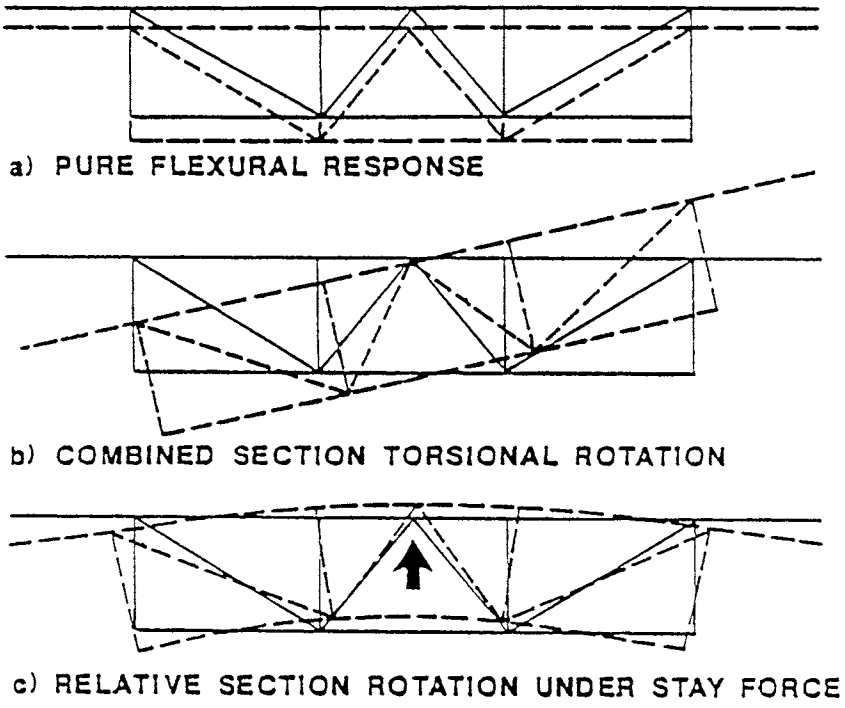

Figure 5. Gross Cross-Sectional Deformation Modes.

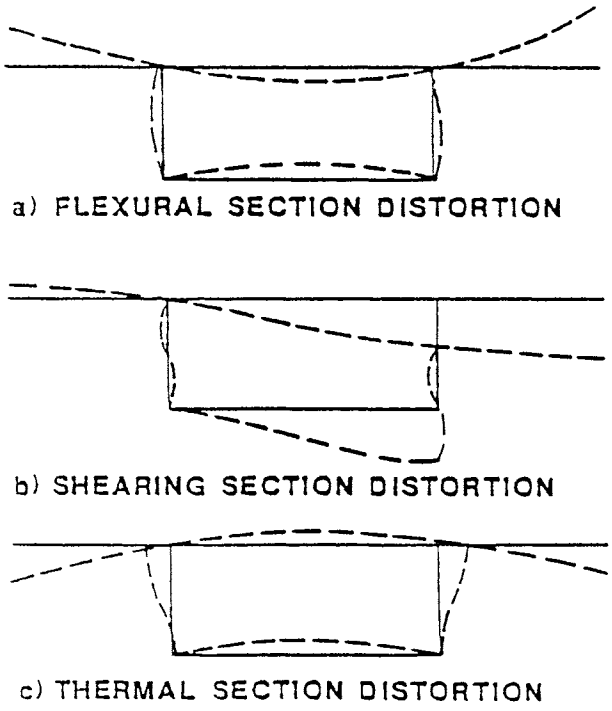

Figure 6. Local Cross-Sectional Distortion Modes.

a single-cell girder in Figure 6. Figure 6(a) shows bending of the cross section attributable to symmetric loading, and Figure 6(b) depicts shearing distortion resulting from antisymmetric (torsional) loads. Figure 6(c) illustrates cross-sectional distortion caused by thermal gradients. This topic is discussed further in the companion report on thermal strains (Duemmel et al., 1992). Cross-sectional distortion leads to a redistribution of stresses, which thereby reduces the section's transverse load distribution capacity. Warping is an out-of-plane displacement of the cross section arising from torsional loading and is composed of torsional and distortional components. Torsional warping causes longitudinal displacements, which are associated with shear deformations in the planes of the webs and flanges. A single-cell, simply supported box girder under torsional loading is shown in Figure 7. Assuming that rigid transverse diaphragms prevent cross-sectional distortion, longitudinal torsional warping displacements occur at all points except at midspan, where the cross section remains plane by symmetry. If the cross section is allowed to distort, additional warping displacements develop as a result of in-plane bending of the flanges and webs. This distortional warping deformation is also shown in Figure 7, and the added twist of the cross section attributable to distortion is shown in Figure 8.

Torsional and distortional warping displacements lead to normal (or warping) stresses when constrained at a continuous or fixed support. These stresses, which depend on the loading, support conditions, and geometry of the structure, may add significantly to bending stresses. Maisel and Roll (1974) indicated that warping

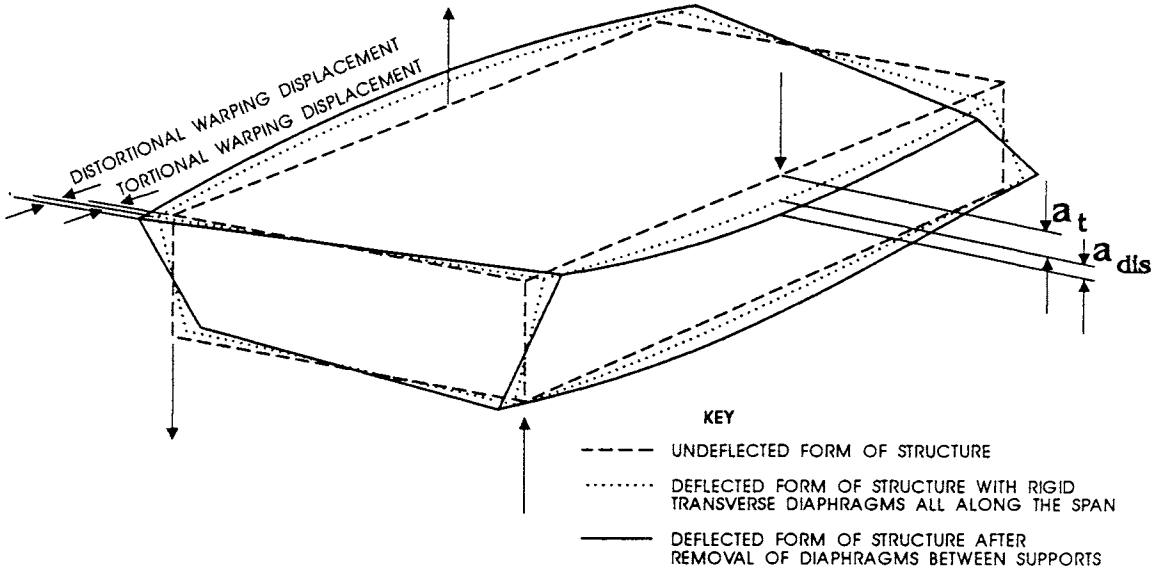

Figure 7. Warping Deformation in Box Girder. a_t = torsional warping; a_{dis} = distortional warping.

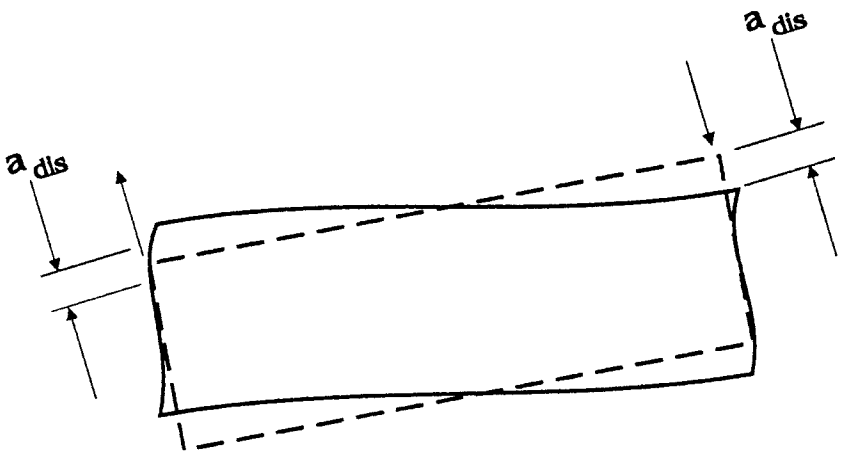

Figure 8. Cross-Sectional Twisting Due to Distortion. a_{dis} = distortional warping.

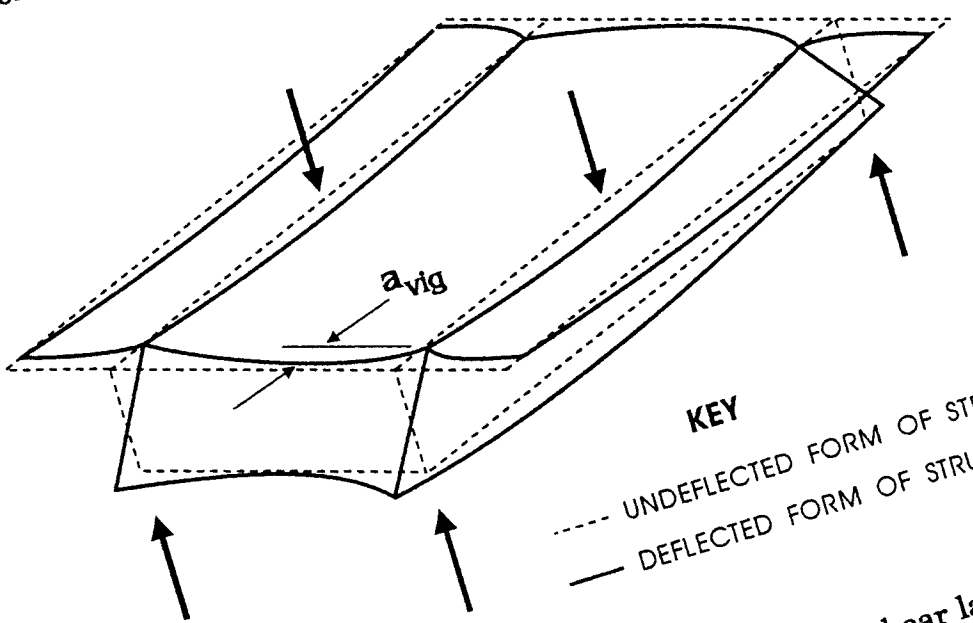

Figure 9. Shear Lag Deformation in Box Girder. a_{vig} = shear lag distortion.

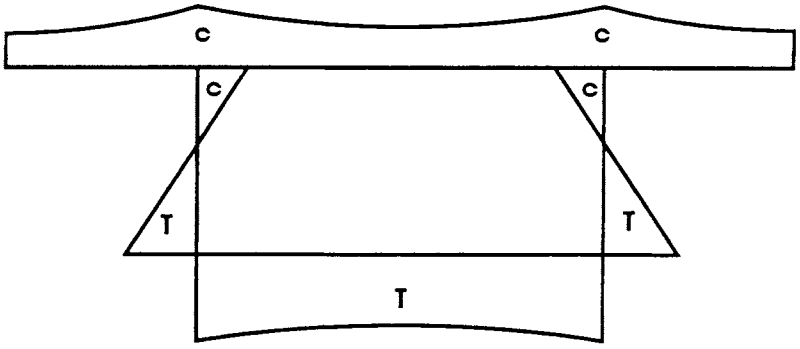

Figure 10. Typical Normal Stress Distribution in Box Girder. T = tension; C = compression.

stresses in concrete box girders are mainly due to distortional warping because torsional warping is limited by the high torsional stiffness of the box section.

Shear lag is a form of warping that arises in box sections subjected to bending without torsion. Figure 9 illustrates the differential longitudinal displacement of points in the cross section resulting from shear deformation in the planes of the flanges. Shear lag deformation causes increased deflections and significantly affects the distribution of normal stress across the width of the flanges, as shown in Figure 10. Bending theory neglects shear lag, and its use leads to underestimation of normal stresses in the flanges. Kristek and Bazant (1987) stated that shear lag effects increase with the width of the box girder and reported that the nonuniformity of the longitudinal stress distribution may be more pronounced in the vicinity of stay reaction forces in cable-stayed bridges. Barton et al. (1990) presented evidence of significant shear lag during construction of the James River Bridge. Reversed or negative shear lag, a phenomenon in which longitudinal normal stresses in the flanges are higher away from the webs, has been investigated by a number of authors (Chang & Zheng, 1987; Foutch & Chang, 1982; Kristek & Studnicka, 1988; Maisel, 1986).

Methods of Mechanical Analysis

The considerable use of box girders in bridges in the past two decades has led to numerous methods for their analysis. Maisel and Roll (1974) conducted an ex-

tensive literature survey and reviewed available analysis methods applied to rectangular, single-cell, straight box girders with uniform cross sections. These methods require the use of only a hand calculator and consider individually the effects of bending, torsion, shear lag, distortion (transverse bending), and torsional and distortional warping. Numerical examples were given for each method, and the effects of each mode of deformation were shown. Maisel (1982) presented an expanded literature survey to include methods of analysis suitable for programming by computer. These included the equivalent beam method, grillage method, folded plate and finite strip analysis, finite element method, transfer matrix method, and thin-walled beam theory. This literature review is comprehensive, and readers are referred to this report for references prior to 1980. The following survey outlines recent developments and trends in the computer analysis of box girders.

Many developments have been made in formulating analysis procedures for box girder bridges over the past decade, and most are a direct result of rapid advances in microcomputer technology. Recent literature reflects increased use of both general purpose and specialized finite element codes because of the versatility and decreased computer costs of the finite element method. Accurate finite strip and folded plate analysis codes have been developed but are often limited to a restricted range of problems. The use of thin-walled beam theory requires much less computer time than three-dimensional finite element analysis, making it useful in the preliminary design stages. A number of approximate methods are available for relatively rapid use by design engineers.

Thin-walled beam theory, based on the generalized coordinate method of Vlasov (1961), has been shown to be an accurate, economical method for analyzing box girders. Maisel (1982) further developed thin-walled beam theory into a matrix formulation for programming on a microcomputer. This method treats the structural responses mentioned, with the added capabilities of analyzing single or multicell sections of rectangular or trapezoidal cross sections. Maisel (1986) extended his earlier work to include a detailed examination of shear lag behavior. Longitudinal stress distributions obtained using thin-walled beam theory compared more closely with results obtained using finite element and finite strip methods than results using classical beam theory. Although this method was shown to be straightforward and accurate, the author stated that box girder bridges with complex geometry or nonuniform cross sections could be better analyzed using box beam finite elements.

Mavaddat and Mirza (1989) programmed Maisel's formulation specifically for the analysis of straight concrete box girders with one to three cells. Although the procedure is limited to simple-span or two-span continuous bridges with concentrated loads at midspan, it can be used interactively on personal computer systems. The analysis is performed in three stages, separately considering the effects of bending and St. Venant torsion, torsional and distortional warping, and shear lag. The analysis results required a relatively short run time and agreed closely with Maisel's calculations. The program's compact formulation is emphasized by decreased computer time and storage requirements, making it advantageous for parametric studies, interactive design procedures, and generation of influence lines.

The use of finite element analyses has increased during the past decade because of falling costs and the increased speed of small computers, along with the availability of general and specialized codes. Scordelis, Watsi, and Seible (1982a&b) used two finite element programs to obtain analytical results for comparison with a large scale model test of a two-span, multicell, skewed concrete box girder bridge. Both SAP, a general purpose three-dimensional frame analysis code, and CELL, a plate element code for analysis of cellular bridge structures, yielded excellent agreement with measured reactions, deflections, and moments.

Evans and Rowlands (1985) used QUEST, a box girder analysis program employing quadrilateral shell elements, to analyze skewed single-celled, single-span box girders. The accuracy of the finite element results was assessed by comparison with several model studies, and it was concluded that reasonable predictions of deflections and longitudinal stresses could be made using a fine mesh. The authors also performed a parametric study of the effects of skew using a shell element model and found that increased skew angle led to significant changes in the longitudinal stress distribution and additional cross-sectional distortion.

Murtuza and Cope (1985) investigated the behavior of two scale models of single-span, reinforced concrete box girder bridges using linear elastic and nonlinear finite element analyses. They found that the linear model could accurately predict reaction forces, but stresses and deflections were greatly underestimated because of the loss of stiffness resulting from concrete cracking. The nonlinear model, based on a simplified material relationship, showed good correlation with experimental results and was able to predict failure modes and loading.

Kuzmanovic and Sanchez (1986) explored the feasibility of using finite element methods to obtain transverse influence lines for load distribution and torque. They found that, although such methods will yield accurate results, the amount of data required to formulate the models limits their usefulness as a design aid. This type of model was better suited to analyzing previously established designs.

Chang and Zheng (1987) investigated the negative shear lag effect in cantilever box girders using a variational approach (principle of minimum potential energy) and the finite element method. Triangular plate elements were used to model a cantilever box girder under a symmetric load. Computed results for transverse distributions of bending stress agreed well with those of the variational method as well as measured results from a Plexiglass model test.

Batla, Reisnour, and Pathak (1984) produced a simplified finite element program (FAP) for analyzing constant depth, box girder structures. Rectangular plate elements were used in which the number of nodal degrees of freedom was reduced from six to four by consideration of the one-way transverse behavior exhibited by folded plate structures. Computer times and memory requirements were greatly reduced, and results obtained using the code showed good agreement with more exact analysis methods.

Specialized box beam finite elements have been developed that have substantially shorter computer run times than rectangular shell elements. Zhang and Ly-

ons (1984) used a box beam element that considered bending, torsion, distortion, and warping response in analyzing curved bridges. Analysis times were approximately one tenth of the time required for plate elements, making this type of element useful in the preliminary design stage.

Mikkola and Paavola (1980) presented a finite element method of box beam analysis based on Vlasov's method of separation of variables. These thin-walled beam elements accounted for the effects of flexure, torsion, cross-sectional distortion, torsional and distortional warping, and shear deformation. A computer program was developed, and results were compared with experimental results and finite strip and folded plate analyses. The authors' method was shown to be reliable in predicting longitudinal stresses and transverse bending stresses but was inaccurate in describing shear stress distributions because of the use of linear warping functions. The authors concluded that the addition of parabolic or cubic warping functions would yield better results and would allow prediction of shear lag effects.

Boswell and Zhang (1984) used a thin-walled box beam element with nine nodal degrees of freedom to analyze the effects of cross-sectional distortion in a number of single and multicell, straight and curved girder bridges. Their results compared favorably with finite element and experimental results.

Chourdhury and Scordelis (1988) formulated a nonprismatic box beam element, based on thin-walled beam theory, for linear elastic and nonlinear finite element analysis. They stated that the simplicity and reduced computational requirements of box beam elements made the elements well suited for nonlinear analyses, which have greater computational time and storage requirements. The elements consider the effects of longitudinal prestress, longitudinal warping, and transverse distortion. Two programs were developed for analyzing curved, prestressed, concrete box girder bridges: LAPBOX for linear elastic analysis, and NAPBOX for nonlinear material analysis. These codes were verified by comparison with results of other analytical methods and experiments, and the nonlinear analysis was shown to be effective in predicting the dominant structural behavior for elastic, inelastic, and ultimate loading stages.

Kanok-Nukulchai and Sivakumar (1988) developed elements for analyzing members with general thin-walled cross sections based on the degeneration concept. They reported that the elements were versatile for modeling detailed cross sections and reduced computational effort since only three "sectional" degrees of freedom were used for all elements of the same cross section. A six-node, thin-walled membrane element was used to model the box girder superstructure of a cable-stayed bridge model. Displacement and stress results compared well with those obtained from experiments and from general shell element analyses.

Razaqpur and Li (1990) derived a box girder finite element model based on an extended version of Vlasov's thin-walled beam theory. The formulation used exact shape functions derived from the governing differential equations, eliminating the need to divide the model into multiple longitudinal elements. This element was applied in the analysis of multicell, multibranch box girders. The results of this

method compared well with three-dimensional shell, finite element results in general, but local effects at the intersection of the three members of multibranch bridges were not accounted for.

Waldron (1986) formulated a general stiffness method for analyzing thin-walled girders of nondeformable cross sections that was suitable for programming by computer. The method could analyze systems of straight or curved box girders using specialized beam elements with 4 degrees of freedom at each node. Element stiffness matrices were derived by inversion of the element flexibility matrices, and expressions for equivalent nodal loads from distributed loads and torques were also developed.

Finite strip and folded plate analysis methods have been widely used and updated because of their improved computational economy over generalized finite element codes. Li, Tham, and Cheung (1988) extended the spline finite strip method in order to analyze curved box girder bridges. Although use of the finite strip method is inexpensive, it is limited to problems with simple geometry and boundary conditions. Here, the more adaptable spline finite strip method was extended into a curvilinear coordinate system. Numerical examples demonstrated the versatility of this method, and the results showed excellent agreement with those of finite element and finite strip methods. The authors also noted considerable savings in computer time.

Loo and Srivanich (1983) proposed a two-step procedure for analyzing cable-stayed box girder bridges with single planes of stay cables. In this method, the structure is first analyzed as an equivalent planar system, using a mixed flexibility and stiffness method, to obtain the stay cable forces. A three-dimensional finite strip analysis of the box girder is then performed using the previously determined cable stay forces as applied loading. The finite strip analysis program used in the second stage employed a general flexibility procedure, which allowed consideration of multispan bridges. A small scale perspex model was built and tested, and measured deflections and strains compared well with those of the proposed method. In addition, the accuracy of the authors' procedure was confirmed by a shell finite element analysis of the test model. A comparison of computer run times indicated the efficiency of the proposed method.

Cheung and Wenchang (1989) formulated a finite strip method for analyzing continuous, haunched box girder bridges. Specialized web and flange elements were developed to model the changes in the cross section of the girders. The results of this modified finite strip analysis compared well with finite element results in numerical examples. The authors stated that their method converged quickly and was more efficient than finite element methods.

Kristek and Studnicka (1988) used folded plate theory to investigate negative shear lag and verified the results of Chang and Zheng (1987). Their method, which employs harmonic analysis, was limited to simply supported girders. The cantilever box girder analyzed in previous studies was modeled as a statically equivalent, simply supported beam, which illustrated the limitations of the method. The results

showed good agreement with those of previous studies. A two-span continuous prestressed box girder was analyzed to show the implications of negative shear lag on practical bridge structures.

Kristek and Bazant (1987) applied a Fourier series solution, extended from folded plate theory, to analyze the effects of shear lag on concrete box girder creep. They stated that this method, developed specifically for analysis of shear lag in box girders, was more efficient than using finite element codes or programs based on more classical folded plate theory. Although this method was most suited to simply supported beams, a continuous girder could be approximated as a system cantilever and simply supported segments. Numerical examples showed that the shear lag effect can significantly increase stresses caused by concrete creep.

Song and Scordelis (1990a) developed a harmonic shear lag analysis using plane stress elasticity, which can be used for simply supported or continuous box girders. The solution was incorporated into a computer program, SHLAG, and comparisons with results from other solutions were presented in examples. This method is simpler than the finite element and folded plate methods, and results compared well with folded plate elasticity solutions. In another report (1990b), the authors derived empirical formulas for longitudinal stresses based on SHLAG results. These results were in agreement with folded plate theory.

A number of approximate analyses have been formulated to give designers reasonable estimates of box girder stresses with minimum time and calculation. Kuzmanovic and Graham (1981) produced a simplified method of shear lag analysis using a variational approach (principle of minimum potential energy) for an idealized cross section. Their results for longitudinal stresses in box girder flanges were reasonable, considering the limited amount of numerical work involved. Kristek and Evans (1985) developed a harmonic analysis for shear lag in single or multicell box girders. Numerical examples and a program for a hand calculator illustrated the use of this method as a design aid.

Ishac and Graves Smith (1985) presented simple design approximations for transverse bending moments in single-span, single-cell, simply supported, rectangular box girders. They used rectangular shell finite elements in a parametric study of three cross sections. A simple framework analysis of the design cross section yielded reference moments, which were related to the finite element results through interpolation functions. The calculated estimates of transverse moments were within 5 percent of the finite element solutions.

Shushkewich (1986) formulated equations for the membrane forces acting within simply supported box girder bridges. The top and bottom flanges, webs, and side cantilevers were considered individually, and the resulting equations yielded forces that were within 3 percent of those predicted by folded plate analysis. Shushkewich (1988) expanded his analysis to determine transverse bending moments and shear forces using a plane frame analysis program in conjunction with the previous equations. Trapezoidal cross sections, point loads, self-weight, and antisymmetric loads were also treated. Results again showed good agreement with folded plate analyses.

METHODS

Overview

A heavily loaded truck was placed at specific locations along the main span and adjacent side spans of the bridge. Strain measurements were recorded in the pylon and box girder segments using the data acquisition system. A detailed finite element model was developed and used as a basis for comparison with the measured response data.

Strain Gage Instrumentation

The instrumentation is summarized here to aid the reader in interpreting the data. Readers seeking further details regarding specifications and installation procedures are referred to the instrumentation plan of Baber and Hilton (1988) and the thesis by Hayes (1988).

An extensive array of electrical resistance strain gages mounted on dummy reinforcing bars were installed during construction. Each strain gage was mounted on a 4-ft length of No. 5 reinforcing bar by use of a high-grade epoxy resin cured at an elevated temperature. The gages were waterproofed by use of a layer of epoxy resin followed by a polysulfide compound designed for protection of electronic equipment. An instrumented reinforcing bar is shown in Figure 11. The gaged dummy rebars were subsequently tied into the deck and pylon segment reinforcing cages prior to their placement into the precasting forms. Lead wires, jacketed with TFE Teflon for waterproofing, were run along the cages to blockouts in the walls of the segments. After the segment was cast and placed, the lead wires were retrieved and connected directly to the data acquisition system.

In the field, changes in temperature result in apparent strains in addition to the mechanical strains measured by the strain gages. To compensate for these temperature effects, 90-degree rosette gages, consisting of gages oriented parallel and transverse to the axis of the bar, were used. The transverse portion of the rosette undergoes a Poisson strain as well as a compensating thermal strain. When the gages were wired in a Wheatstone half bridge, a small temperature correction appeared but was not significant for the range of temperatures expected during the study.

The gages were mounted along the curve of the rebar rather than on a flat surface, which would have necessitated extra machining. Although mounting the gages on a curve avoids the uncertainties in strain measurement associated with a reduction of bar area, an additional temperature-induced strain is introduced by the curvature of the transverse gage. This apparent strain is a function of the radius of the curved surface, the thicknesses of the gage backing and adhesive, and temperature change. An approximate correction was given by Measurements Group, Inc. (1983) as:

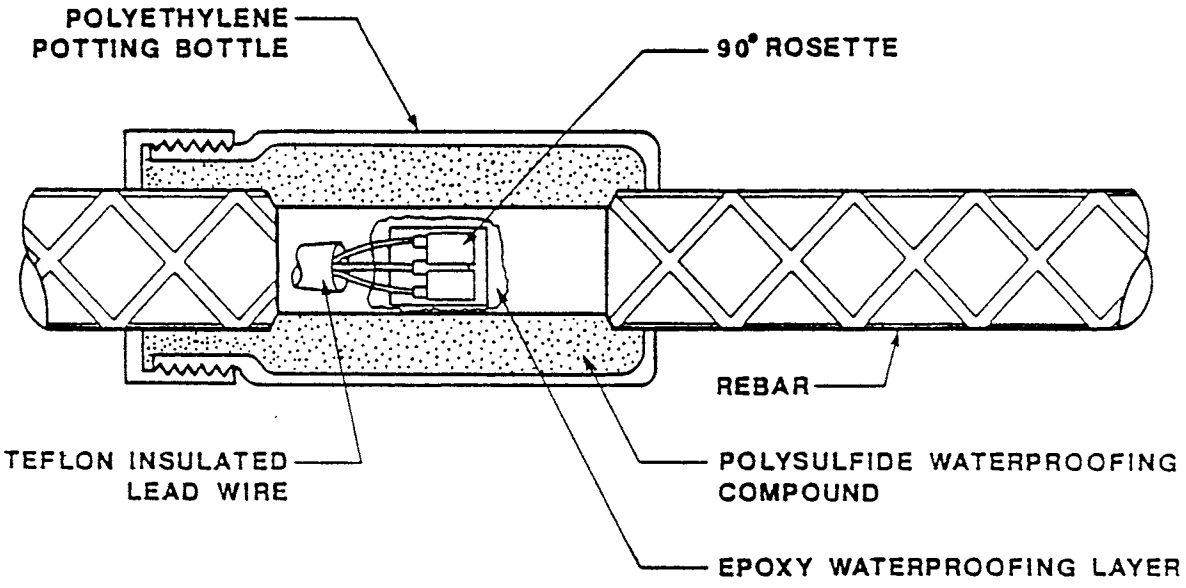

Figure 11. Instrumented Dummy Reinforcing Bar.

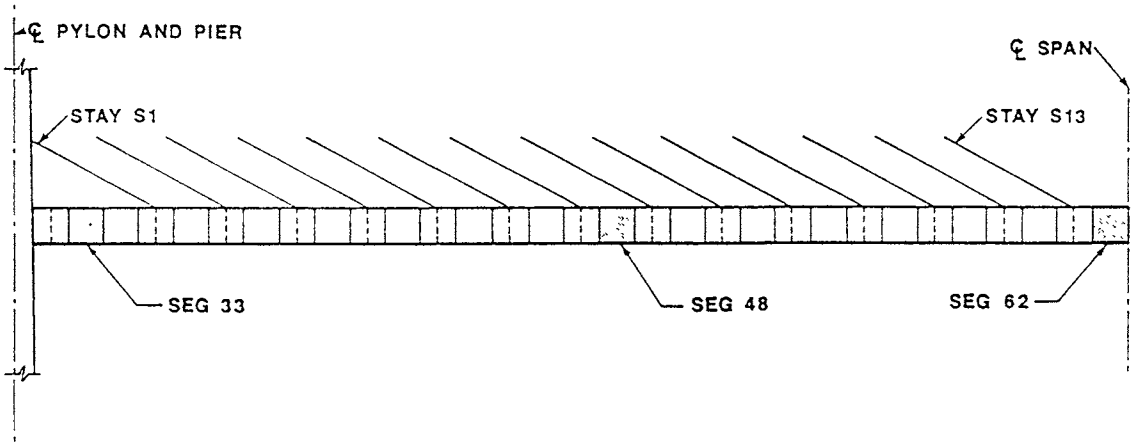

Figure 12. Location of Box Girder Segments Instrumented with Strain Gages.

$$\Delta\epsilon_{APP} = \frac{1}{R}[(1 + 2\nu_{A-B})(h_A\alpha_A + h_B\alpha_B) - 2\nu_{A-B}\alpha_S(h_A + h_B)]\ \Delta T \qquad [1]$$

where ϵ_{APP} = apparent strain induced by curvature

R = radius of curvature

ν_{A-B} = Poisson's ratio of adhesive and backing

h_A, h_B = adhesive and backing thickness, respectively

α_A, α_B = thermal expansion coefficients of adhesive and backing, respectively

α_S = thermal expansion coefficient of specimen

ΔT = temperature change.

Strain gages were installed in three deck segments located in the main span of the bridge. Specifically, the north and southbound lanes of main-span box girder segments 33, 48, and 62 were instrumented with single longitudinal gages and three gage rosettes. Figure 12 shows the locations of the instrumented segments with respect to the south pylon/pier and the center line of the main span. It can be seen that segment 33 is adjacent to the pier, segment 48 is near the quarter span, and segment 62 is at midspan. The locations of the strain gages within each of the segments are shown in Figure 13, where a *dot* represents a gage oriented parallel to the long axis of the bridge, and an *R* represents a strain rosette. The rosettes consist of three gaged rebars arranged at 45-degree angles, which were designed to measure shear strains. Rosette gages were placed in the webs of each instrumented segment. As can be seen in Figure 13, additional rosettes were placed in the top and bottom flanges of segment 33. Readers will wish to refer to Figures 12 and 13 to assist in interpreting the discussion of the field study data.

In view of the complexity of behavior anticipated for box girders, complete instrumentation was not feasible, so the strain gages were arranged to provide data concerning the gross cross-sectional deformations only. The instrumented segments were not connected to delta frames so as to avoid the local cross-sectional distortions likely in these areas. The gage pattern shown in Figure 13 allows for determination of the gross cross-sectional flexure and shear acting in the four webs. The additional rosettes in the flanges of segment 33 serve to provide additional information concerning the torsional shear strains at that location.

In addition to the box girder sections, two sections of the south pylon were instrumented with strain-gaged reinforcing bars. The gages were placed vertically in the uppermost cast-in-place section, just above deck level, and in precast segment D6, located beneath cable stay S7. The locations of these sections are shown in Figure 14. Figure 15 depicts the locations of the strain gages within the instrumented pylon segments. Readers will wish to refer to Figures 14 and 15 to assist in interpreting the field study data.

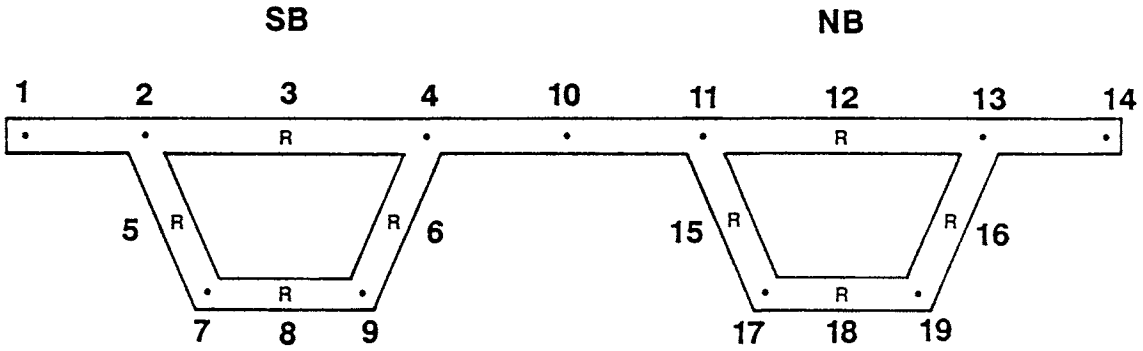

SEG 33

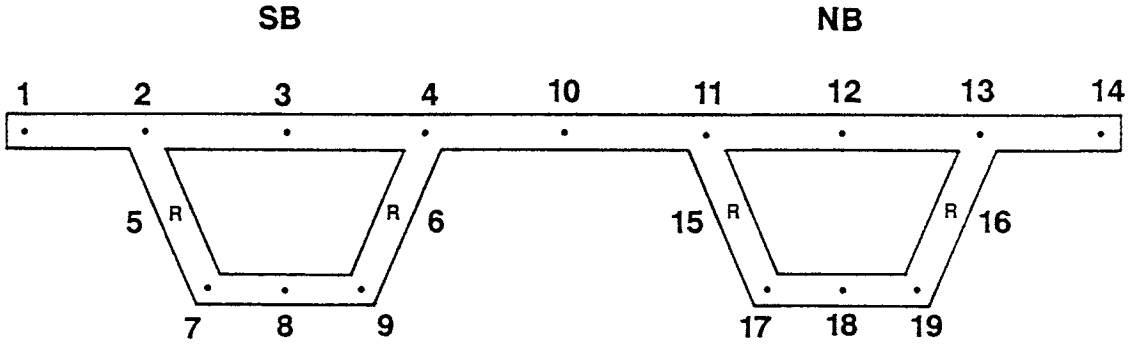

SEG 48 & SEG 62

Figure 13. Location of Strain Gages in Instrumented Box Girder Segments. SB = southbound; NB = northbound; • = gage oriented parallel to the long axis of the bridge; R = strain rosette.

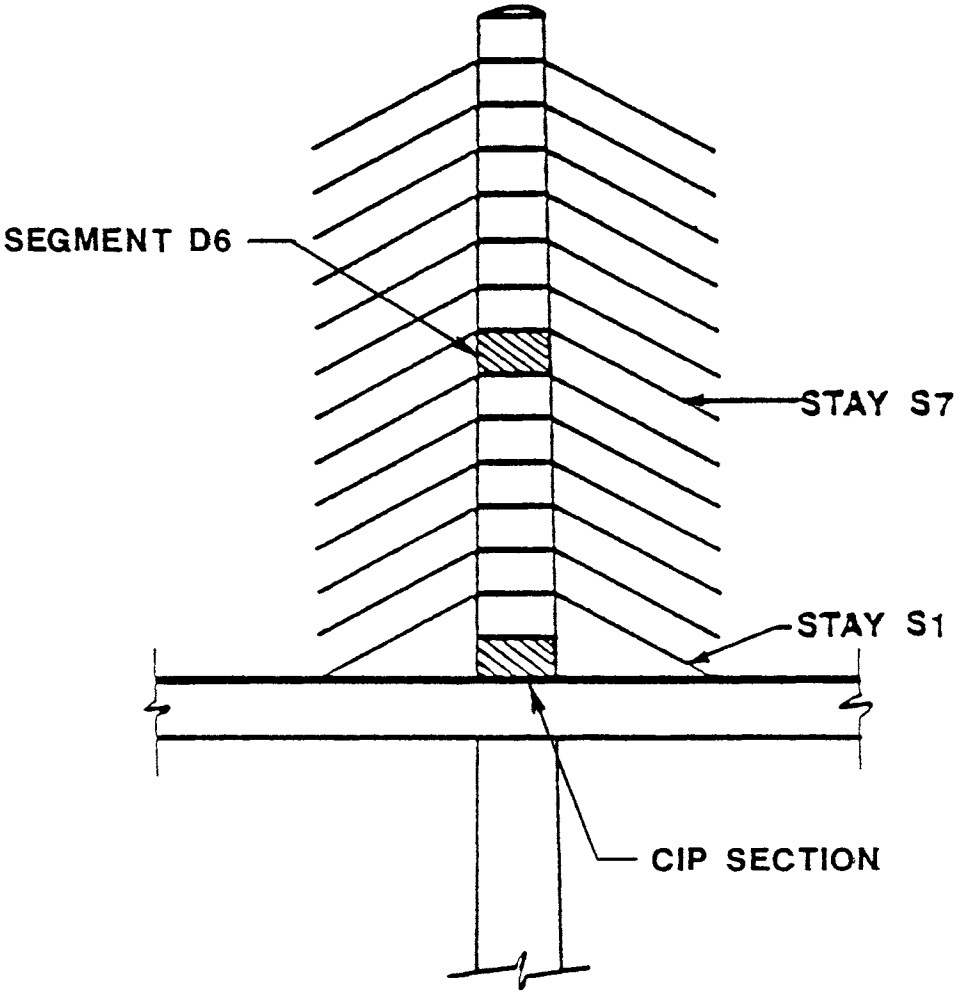

Figure 14. Location of Pylon Segments Instrumented with Strain Gages. CIP = cast in place.

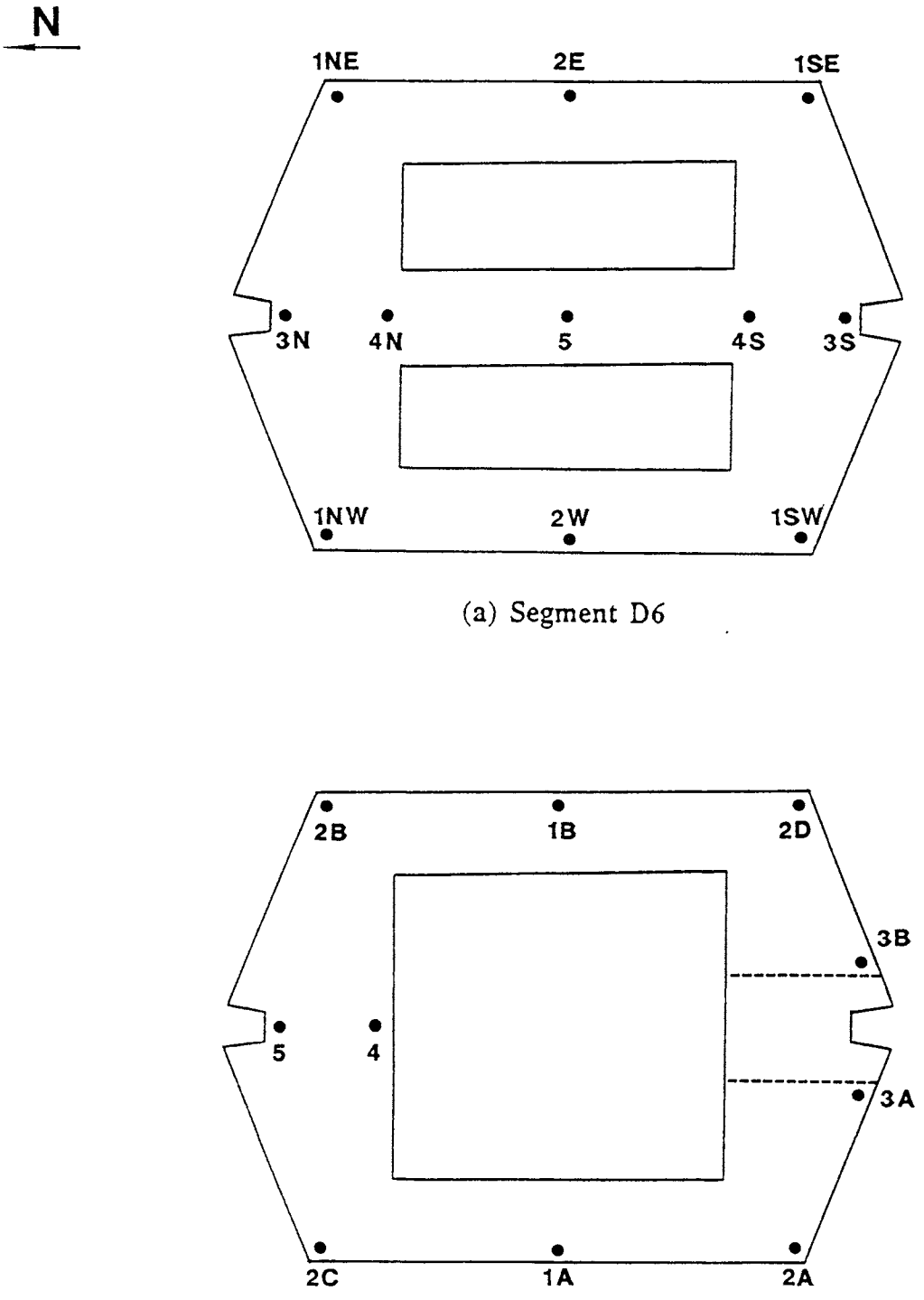

Figure 15. Location of Strain Gages in Instrumented Pylon Segments. CIP = cast in place.

Data Acquisition System

A distributed data acquisition system consisting of several small scanning units linked to a controller by data transmission lines was used. In this system, which is shown schematically in Figure 16, strain gages and thermocouples located in each instrumented section of the bridge were connected to individual scanning units, which in turn were connected to the controller via data lines. This eliminated the need for all data channels to be connected at a single location. The data were then returned by the controller and logged to the hard drive of a portable IBM-compatible personal computer.

The data acquisition system was manufactured by the John Fluke Company. The system uses a Helios main controller to communicate with the remote scanning units located in the instrumented bridge segments. The Helios system will read thermocouples and electrical resistance strain gages in various configurations, each requiring a single data acquisition channel. The data are then stored on a Compaq portable computer in Lotus 1-2-3 format by means of Helios Toolbox data acquisition software. The system uses 110-volt line power via an uninterruptible power supply (UPS), which provides surge protection and a backup power source. The main controller unit, data logging computer, and UPS are protected in an enclosure cabinet with heating and air conditioner units to maintain operational temperature and humidity limits.

Loading

The bridge deck was loaded with a tandem-axle dump truck loaded to the legal maximum. The truck, weighed prior to the test, had a total weight of 49,720 lb, with 16,820 lb and 32,900 lb on the front and rear axles, respectively. The axle loads and dimensions between the front and rear wheels are shown in Figure 17. The truck was placed at 14 locations along the bridge, 1 in each of the four adjacent approach spans and 10 in the main span. These longitudinal load locations are shown in Figure 18, where the number at each load position corresponds to the span number and, within the main span, to a particular position within the span. The instrumented segments were located on the south half of the main span, as shown in Figure 12. For convenience, these sections are shaded in Figure 18 as well. The truck was consistently headed in a southerly direction and positioned such that the center line between the two rear axles was aligned with points where the cable stays were connected to the box girder. The positioning was chosen primarily for convenience to allow precise referencing of the position for use in comparative computational modeling.

At each longitudinal location, there were four transverse load positions. These transverse positions correspond approximately to the interior and exterior traffic lanes of the north and southbound portions of the twin box girder. As shown in Figure 19, the transverse load positions were directly above the webs of the box girders. During the test, strains were recorded with the truck positioned in the

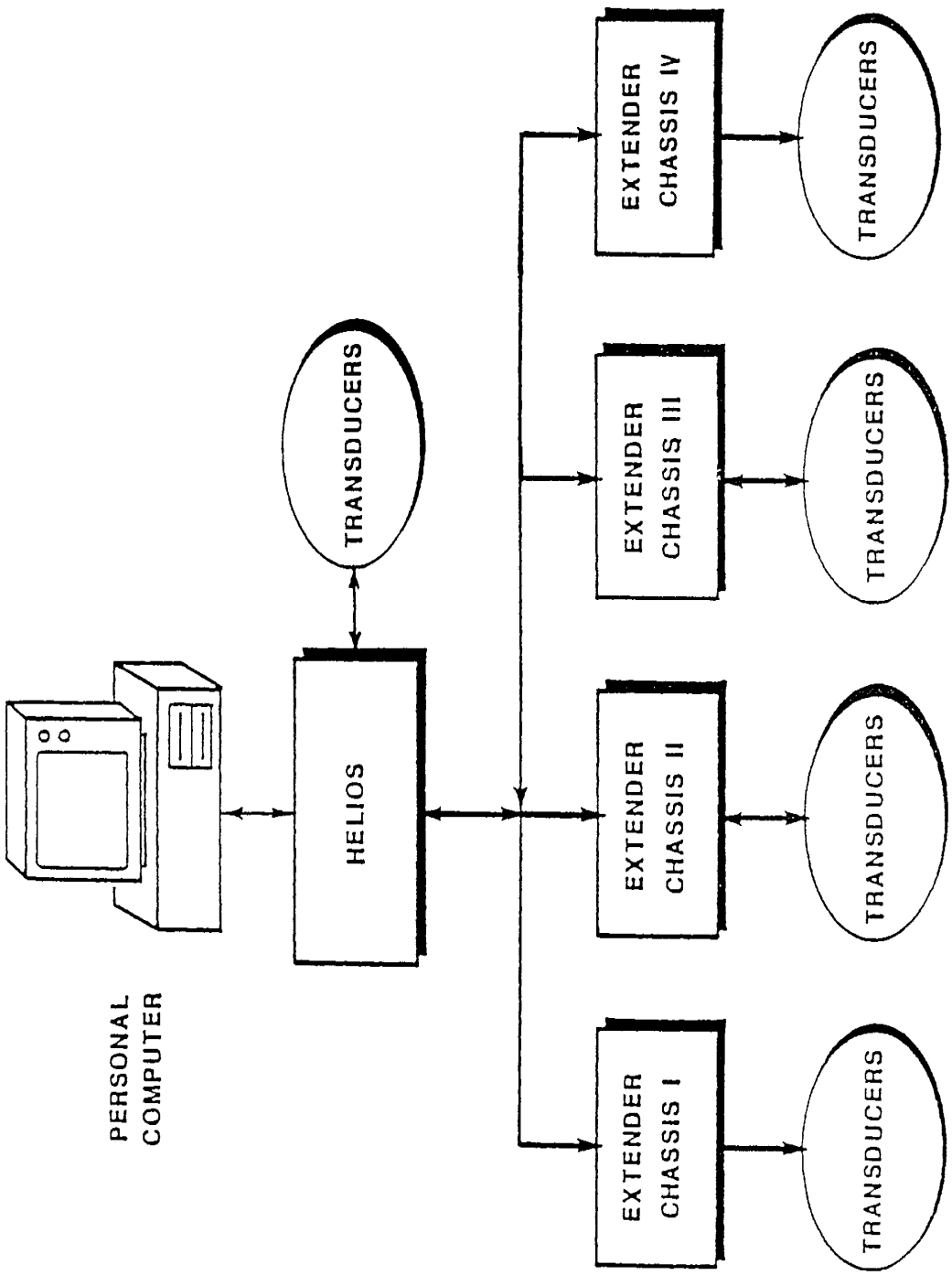

Figure 16. Data Acquisition System.

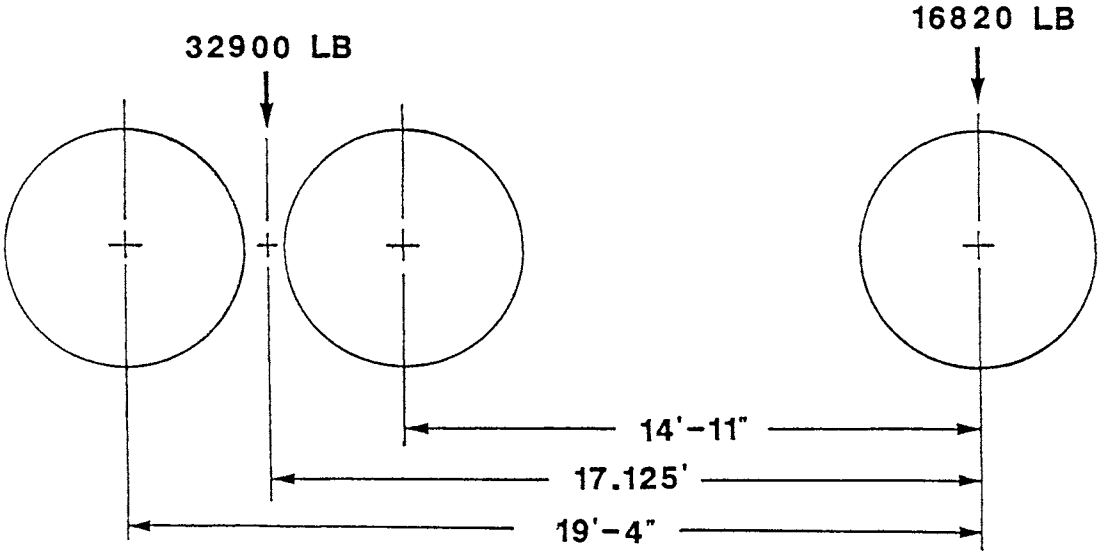

Figure 17. Test Vehicle Dimensions and Loads.

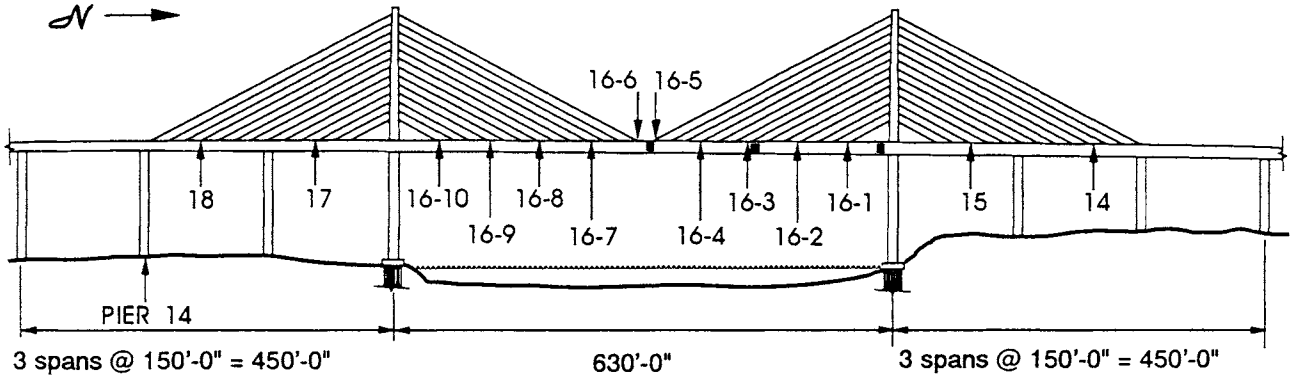

Figure 18. Elevation View of the I-295 Bridge Showing Longitudinal Locations of the Test Vehicle.

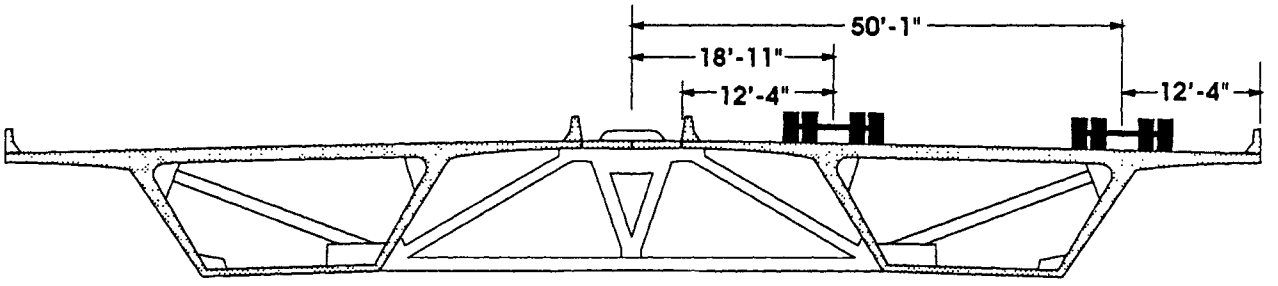

Figure 19. Cross Section of Twin Box Girder Showing Transverse Locations of Test Vehicle.

interior and exterior northbound lanes of the bridge at each of the 14 longitudinal load locations. Strain measurements were taken at only 6 longitudinal locations within the main span when the truck was positioned in the southbound lanes. The data from these load locations were used to validate the majority of the data taken with the vehicle in the northbound lane.

Zero readings for the strain gages were recorded with the vehicle completely off the bridge prior to and at six approximately equal intervals during the test. Because of variations in temperature over the course of the testing, there were slight differences between zero readings, and it was assumed that the small variation between readings was linear. At least two complete sets of strain data were recorded at each load position. The strains caused by the application of the loads were calculated as the difference between the recorded strain and the zero reading calculated at the time at which the vehicle was placed into position. Assuming that the strains in the top and bottom flanges were uniaxial in nature, stresses resulting from the load application could then be calculated by multiplying the incremental strains by a concrete modulus of approximately 4.5 million psi.

Finite Element Model

A finite element model of the bridge was developed for comparison with the strain values obtained in the field test. Although considerable strain response data

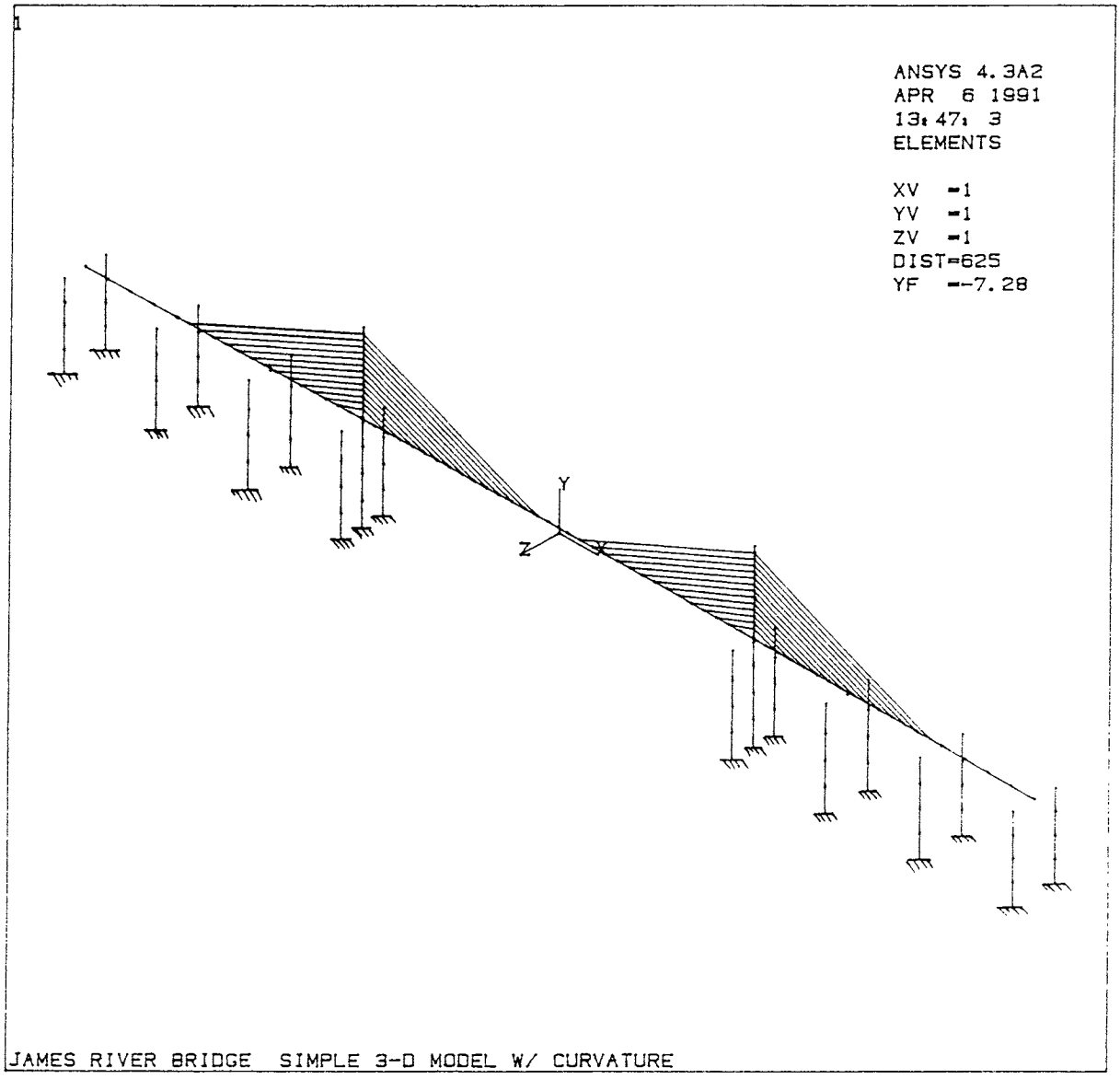

Figure 20. I-295 Bridge Finite Element Model.

were recorded during the test, they represent a single vehicle load positioned at a few locations and provide only a limited picture of the overall behavior of the structure. Hence, the computer model could also be used to predict stresses under a variety of load conditions.

The finite element model used for the live load study was originally developed by Lissenden (1988) for a dynamic study of the James River Bridge. Minor modifications were made to allow for static analysis using P.C. ANSYS V4.3. The model, shown in Figure 20, was three dimensional, in which the twin box girder, pylons, and piers were represented as a series of beam elements. The cable stays were modeled as truss elements. Bridge member properties were used to define the properties of the elements. Loadings were applied to the model as concentrated forces and moments, representing the axle loads of the test vehicle, at the locations corresponding to the longitudinal load positions.

RESULTS

Strain Measurements

Measured Longitudinal Strain Response

Evaluation of the recorded strain data indicated that a significant amount of data were unreliable and had to be discarded. A majority of the gages in segment 33, near the pier, were controlled by an excitation board in the data acquisition system that was found to be defective. As a result, only the three gages in the bottom flange of the northbound portion of this segment recorded reliable data (see Figure 13). The strain data recorded from quarter-span segment 48 underwent seemingly random oscillations that were consistent between gages, suggesting a malfunction in the data acquisition chassis that controlled these gages. The data recorded at midspan segment 62 did not show the unrealistic variations in strain exhibited by the gages in the other sections. Thus, only the strain data from the operational gages in segment 62 and the three reliable gages in segment 33 are discussed here.

Strain data recorded from gages 17, 18, and 19, located in the bottom flange of the northbound lane of segment 33, are presented in Figures 21 and 22 for the test vehicle in the exterior and interior traffic lanes of the northbound box girder. These plots depict the measured strains as a function of vehicle position, measured from pier 14 (see Figure 18). This reference point represents the end of the first span in which the load was placed. The first load point, for example, was at midspan of span 18 and is thus plotted at a distance of 75 ft from the origin. Figures 21 and 22 show that the strains measured at segment 33 were negligible when the test vehicle was in the approach spans. When the truck moved onto the main span, larger strains were consistently recorded in all three gages. The measured strain responses were of the form that could be expected for segment 33, which is located adjacent to the south pier, in the negative moment region of the main span. With

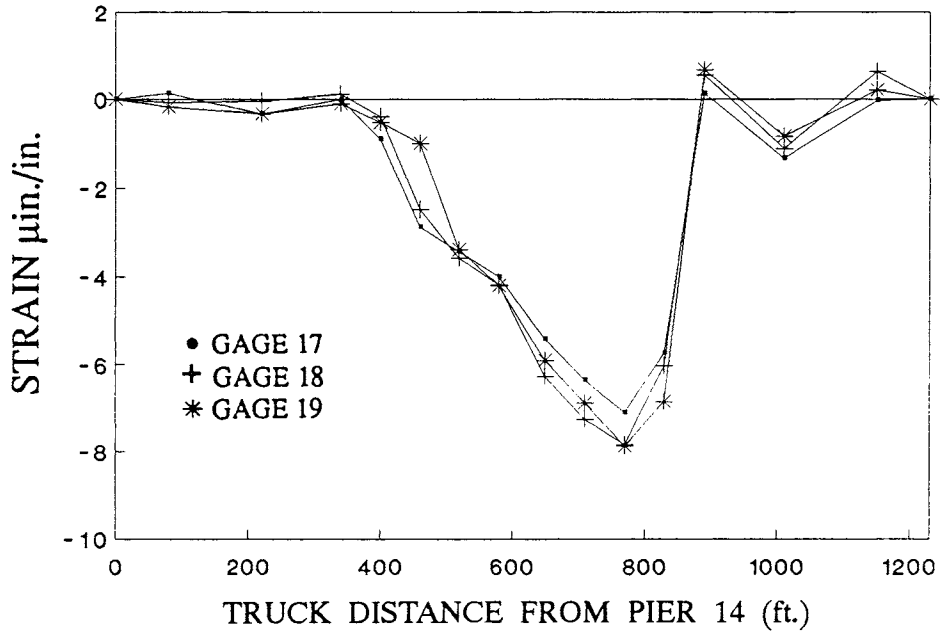

Figure 21. Lower Flange Strains, Segment 33 (Northbound Lane), Vehicle Locations in Northbound Exterior Lane.

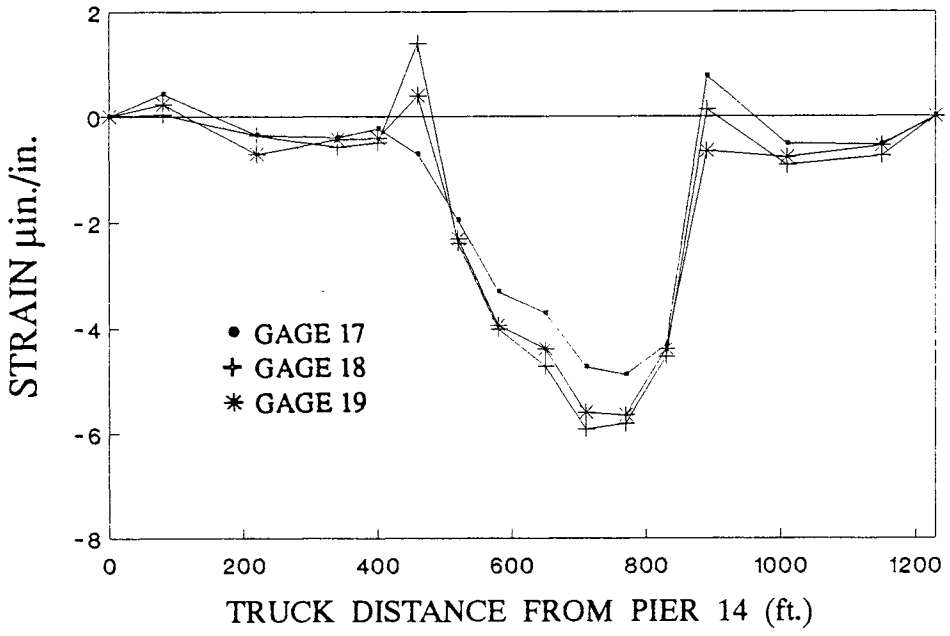

Figure 22. Lower Flange Strains, Segment 33 (Northbound Land), Vehicle Locations in Northbound Interior Lane.

the vehicle in the exterior lane, a maximum strain of about 8.0 microstrains was recorded. The variation of strain as a function of load position was the same with the vehicle in the interior lane, but the maximum recorded strain value was approximately 6.0 microstrains.

Figures 23 and 24 show strains recorded by gages 17, 18, and 19 in segment 33 with the test vehicle positioned in the exterior and interior southbound lanes, respectively. As mentioned previously, strain readings were taken at only six longitudinal load locations when the truck was positioned in these lanes. An examination of these plots shows that the trends in measured strain response were similar to those observed when the test vehicle was in the northbound lanes. The strain magnitudes, however, were noticeably smaller. In this case, the gages were located in the unloaded side of the twin box girder. A maximum compressive strain of approximately 2.0 microstrains was recorded with the vehicle located in the exterior southbound lane, farthest from the gages. With the vehicle in the interior southbound lane, a maximum compressive strain of approximately 3.5 microstrains was recorded. This indicates that, near the piers, a larger portion of the load was carried by the box girder on which the load was placed and the transverse load distribution decreased away from the load.

Strains measured in the top flange of segment 62 are plotted as functions of load position in Figures 25 through 28.Figure 25 represents the strain response measured by gages 1 through 4 of this segment with the test vehicle located in the exterior, northbound traffic lane. Figure 26 shows the same data measured by gages 11 through 14. Figures 27 and 28 present strain data for the same gages as Figures 25 and 26, respectively, but for the test vehicle in the interior, northbound lane. Compared with the data from segment 33, these plots show more scatter between gages, but the magnitudes of the variations were less than 1.0 microstrain. The trends in strain response, however, were relatively consistent. As was shown previously in Figure 12, the gages in this segment were located within a few feet of midspan, and the compressive strains resulting from the load at midspan were expected. The magnitudes of the maximum compressive strains were on the order of 1.0 to 1.5 microstrains and were considerably smaller than expected.

Figures 29 through 32 present measured strain data for the top flange gages in segment 62 with the test vehicle positioned in the southbound exterior and interior traffic lanes. Figures 29 and 31 show the strain response measured by gages 2 through 4 with the truck in the exterior and interior lanes, respectively. Figures 30 and 32 represent the strains recorded from gages 11 and 13 for the same respective load locations. Gages 1, 12, and 14 showed unreliable zero readings during the time at which this portion of the test was conducted, so the data from these gages were not usable. These plots show similar magnitudes of compressive strains as those measured with the test vehicle in the northbound lane, but with less scatter between gages. This would again seem to attest to the validity of the small strain values since similar strain magnitudes were reproduced under separate applications of the load.

Strain data from gages located in the lower flanges of segment 62 are shown as functions of load position in Figures 33 through 36. Figures 33 and 35 present

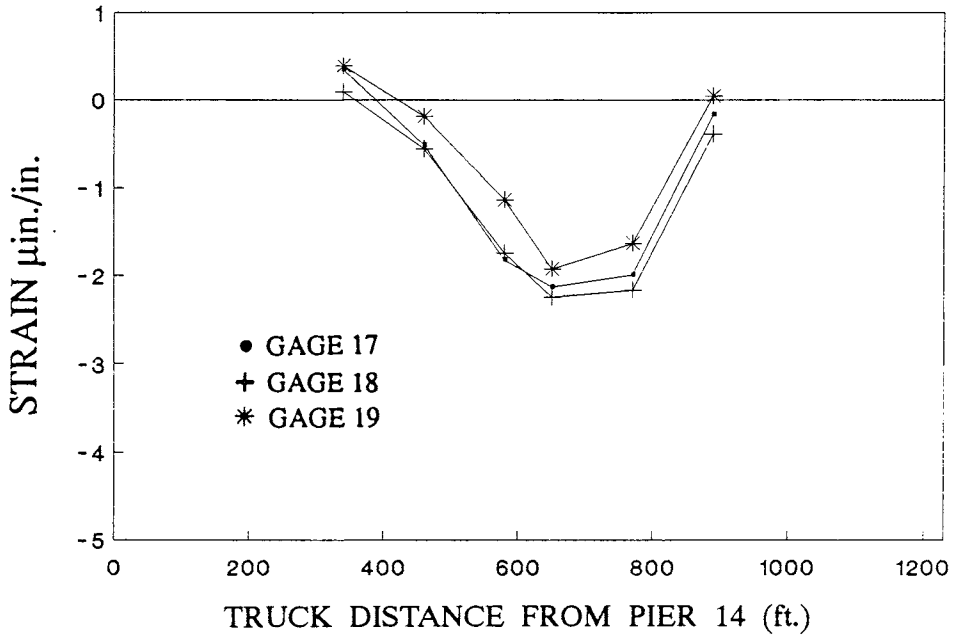

Figure 23. Lower Flange Strains, Segment 33 (Northbound Lane), Vehicle Locations in Southbound Exterior Lane.

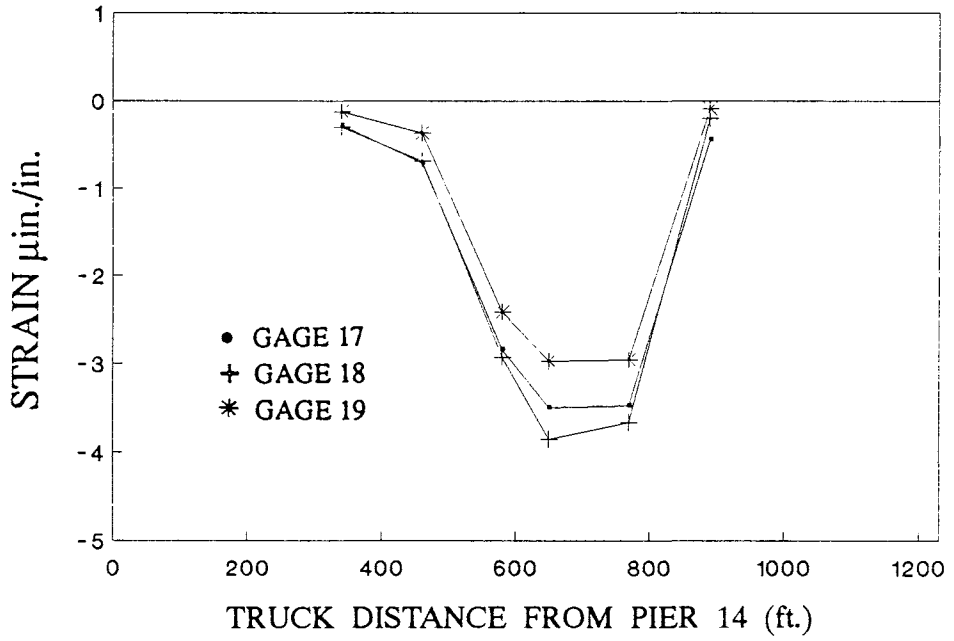

Figure 24. Lower Flange Strains, Segment 33 (Northbound Lane), Vehicle Locations in Southbound Interior Lane.

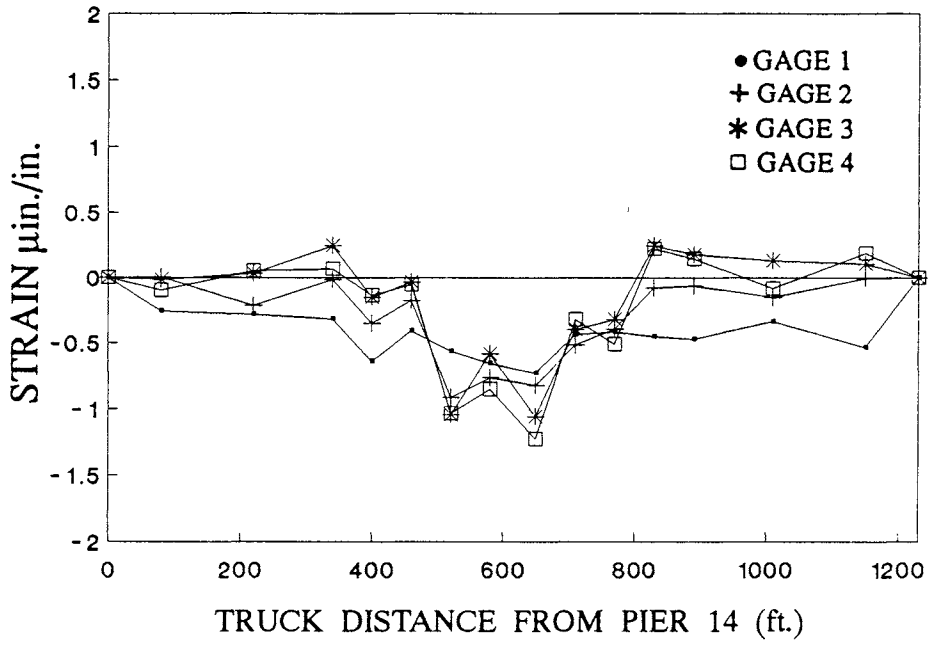

Figure 25. Upper Flange Strains, Segment 62 (Northbound Lane), Vehicle Locations in Northbound Exterior Lane.

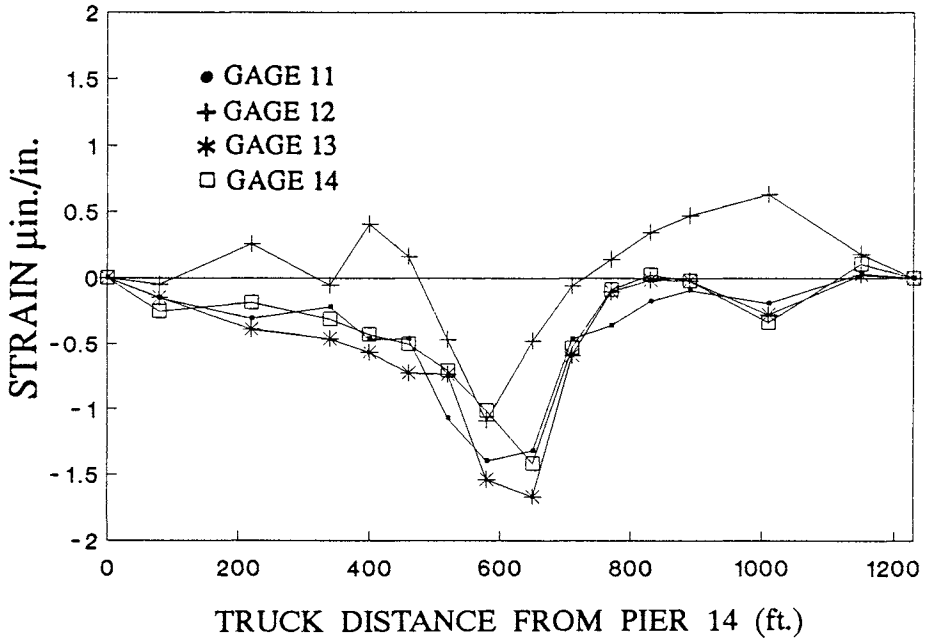

Figure 26. Upper Flange Strains, Segment 62 (Southbound Lane), Vehicle Locations in Northbound Exterior Lane.

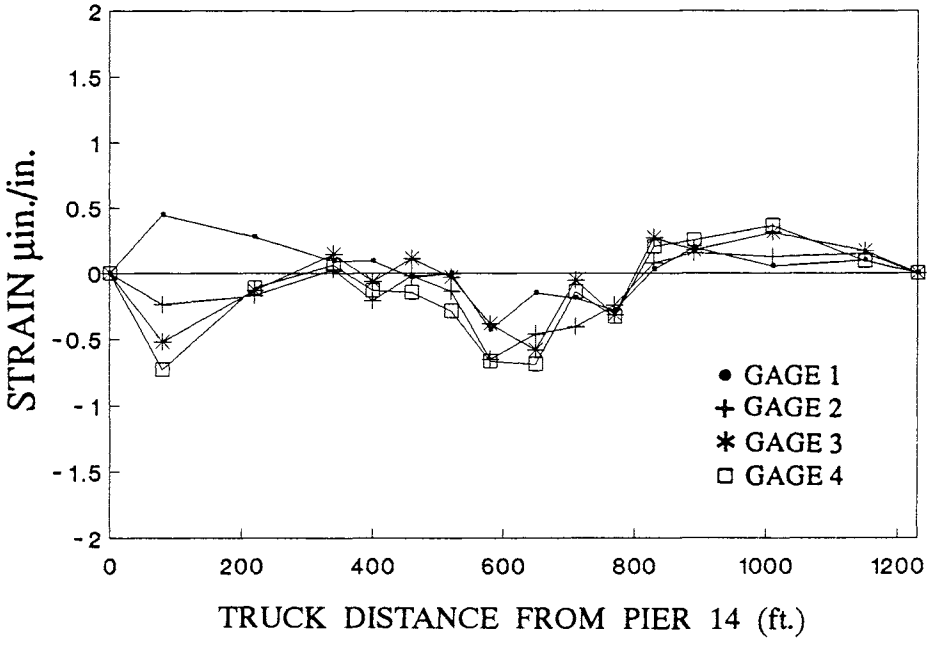

Figure 27. Upper Flange Strains, Segment 62 (Northbound Lane), Vehicle Locations in Northbound Interior Lane.

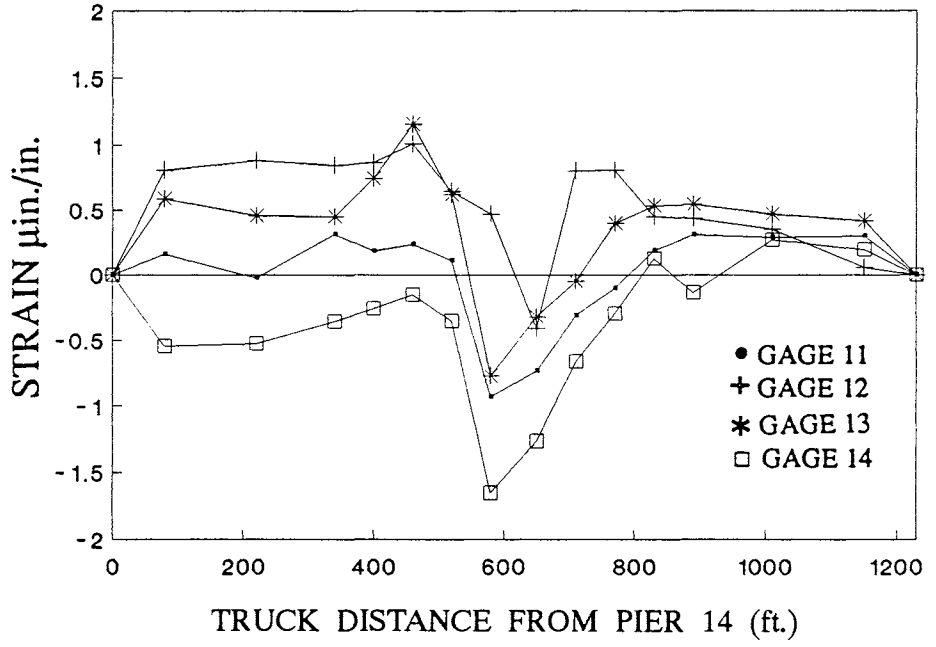

Figure 28. Upper Flange Strains, Segment 62 (Southbound Lane), Vehicle Locations in Northbound Interior Lane.

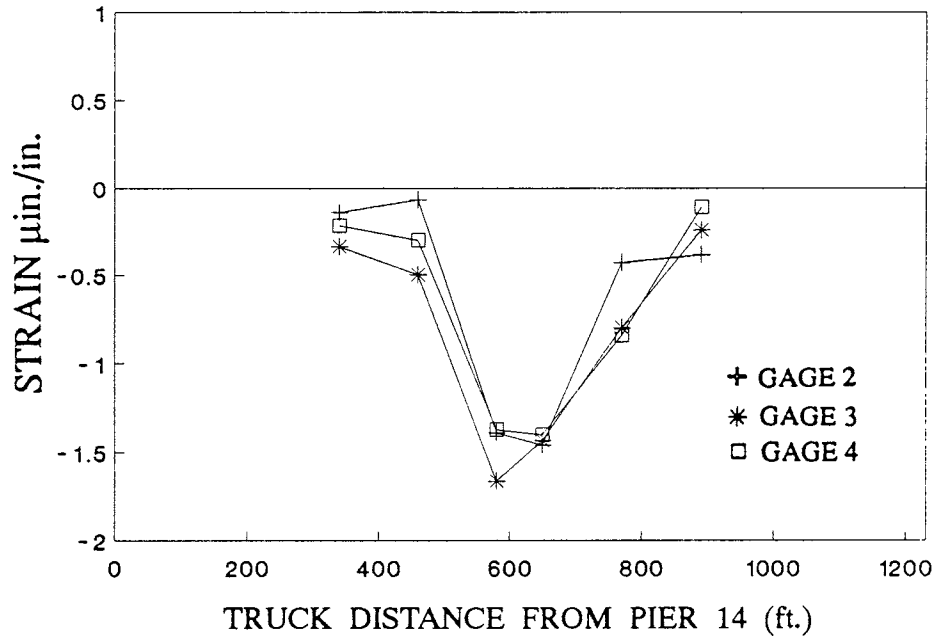

Figure 29. Upper Flange Strains, Segment 62 (Southbound Lane), Vehicle Locations in Northbound Exterior Lane.

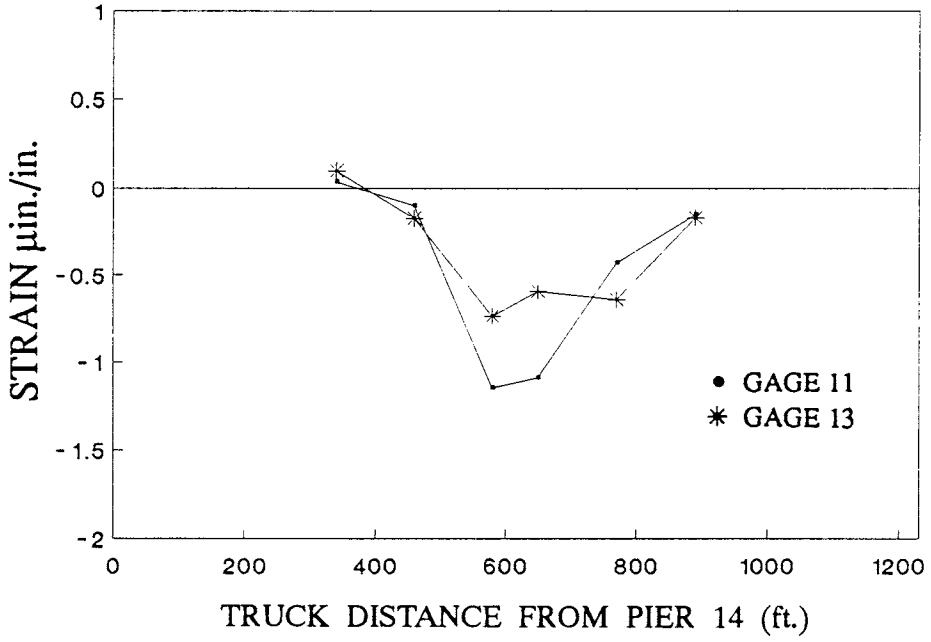

Figure 30. Upper Flange Strains, Segment 62 (Northbound Lane), Vehicle Locations in Southbound Exterior Lane.

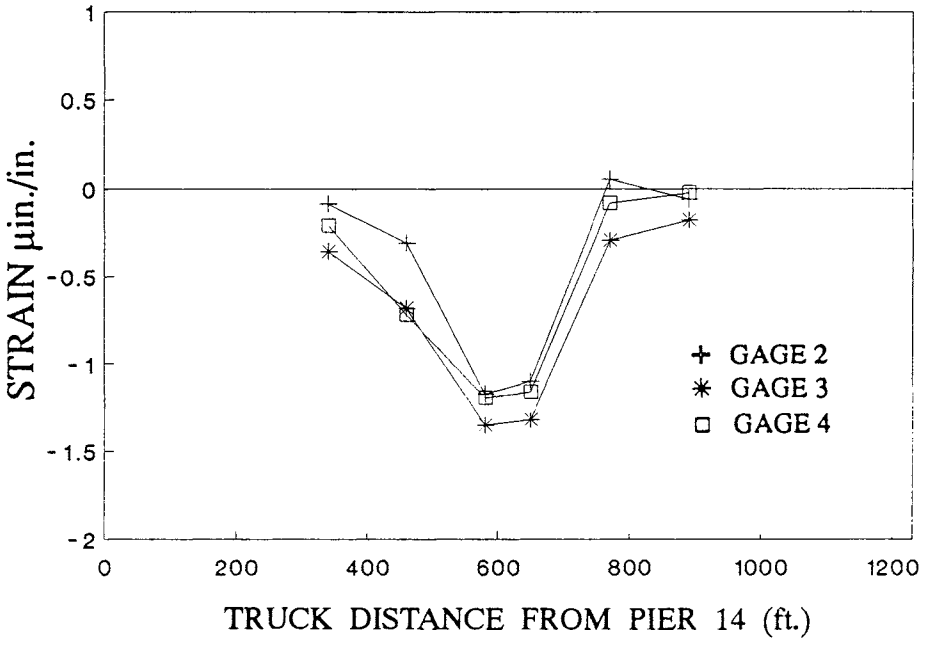

Figure 31. Upper Flange Strains, Segment 62 (Southbound Lane), Vehicle Locations in Southbound Interior Lane.

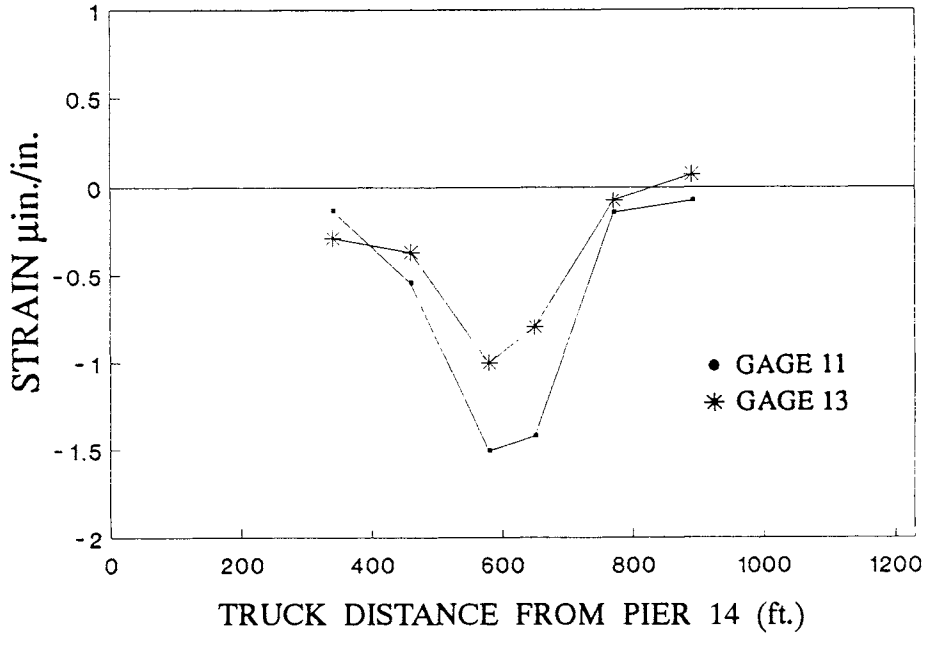

Figure 32. Upper Flange Strains, Segment 62 (Northbound Lane), Vehicle Locations in Southbound Interior Lane.

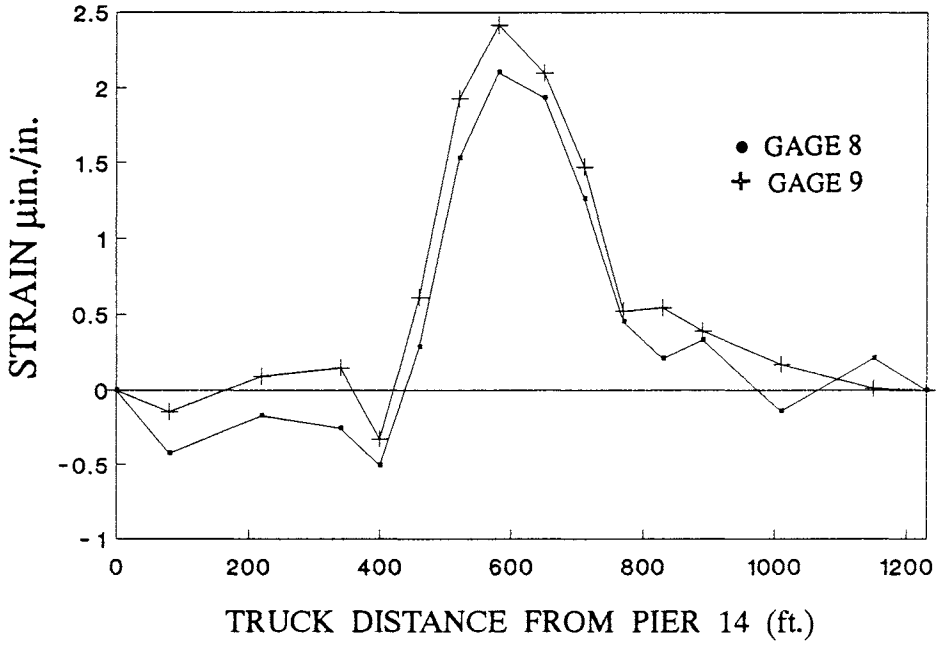

Figure 33. Lower Flange Strains, Segment 62 (Northbound Lane), Vehicle Locations in Northbound Interior Lane.

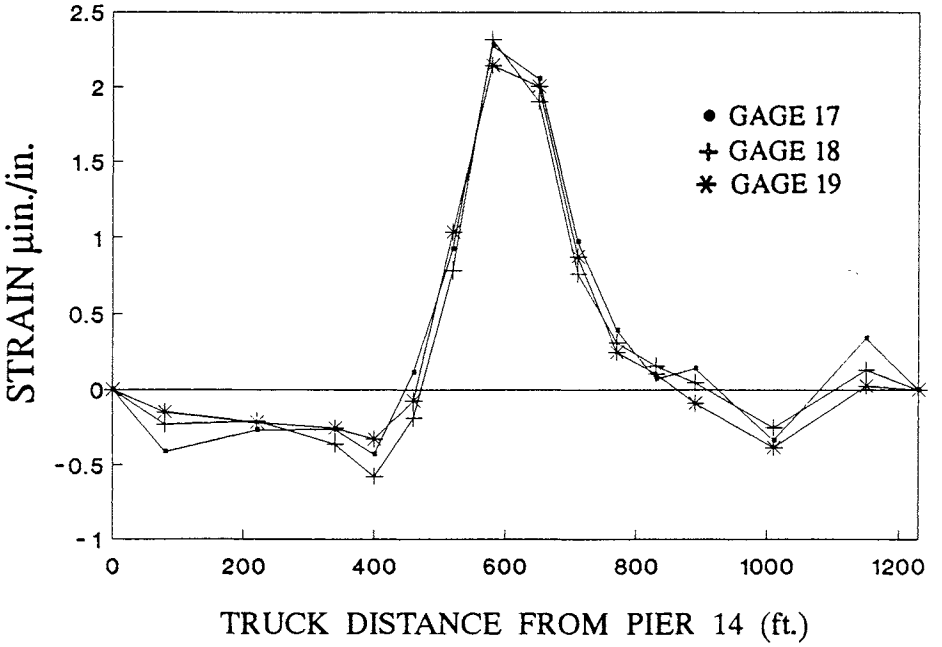

Figure 34. Lower Flange Strains, Segment 62 (Southbound Lane), Vehicle Locations in Northbound Exterior Lane.

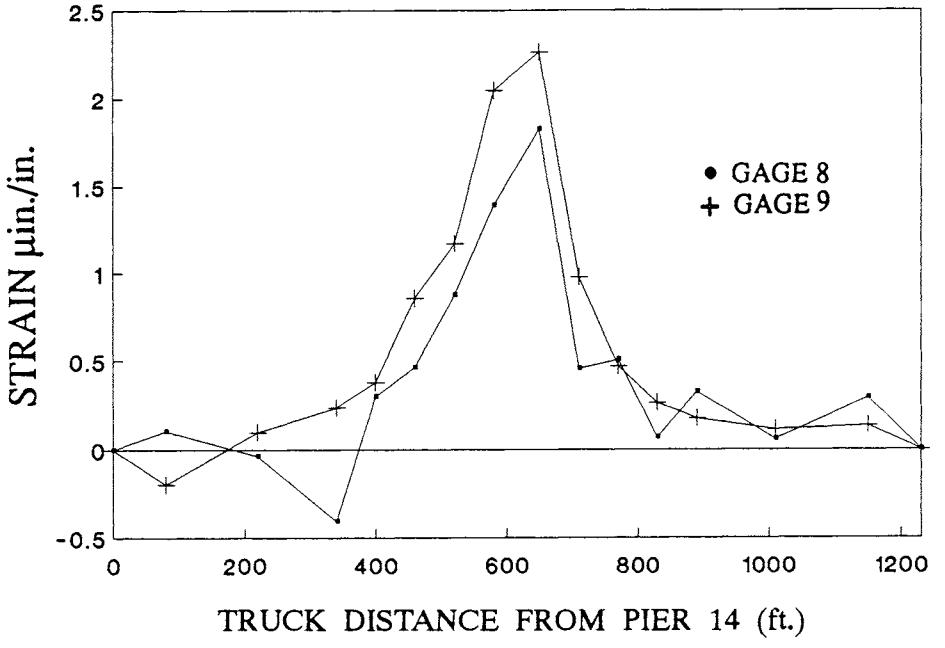

Figure 35. Lower Flange Strains, Segment 62 (Northbound Lane), Vehicle Locations in Northbound Interior Lane.

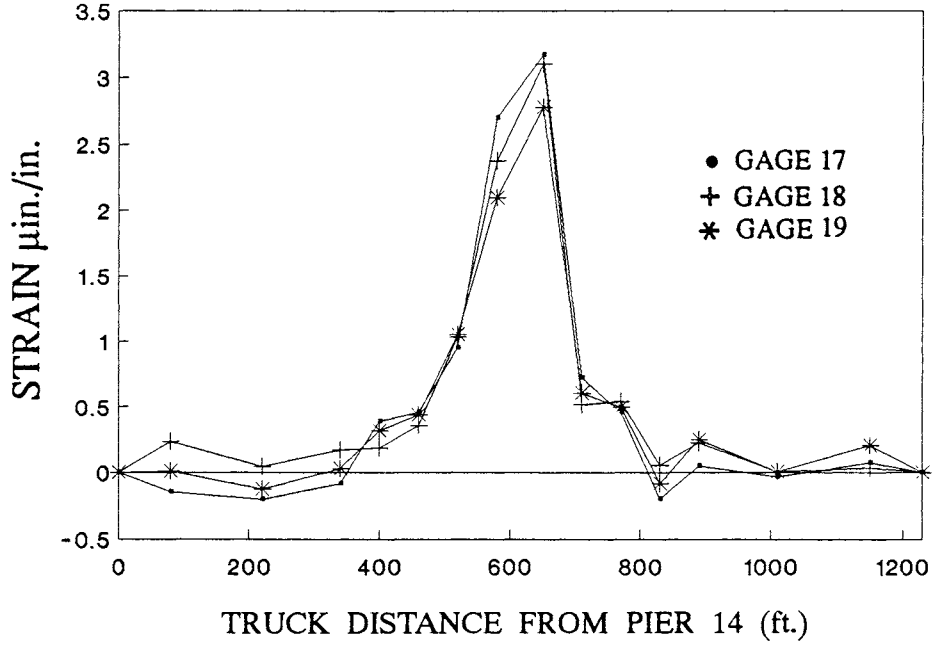

Figure 36. Lower Flange Strains, Segment 62 (Southbound Lane), Vehicle Locations in Northbound Interior Lane.

strain data recorded by gages 8 and 9 in the northbound portion of the box girder resulting from the test vehicle positioned in the exterior and interior northbound traffic lanes, respectively. Figures 34 and 36 provide the same data for gages 17, 18, and 19 located in the lower flange of the southbound portion of the segment. Each of these plots shows the same general trend in the variation of strains, with negligible strains recorded when the test vehicle was located in the approach spans and larger tensile strains measured as it was positioned along the main span. Gages 8 and 9, located in the unloaded side of the bridge, recorded maximum strains of approximately 2.0 to 2.5 microstrains. Gages 17, 18, and 19 in the loaded side recorded maximum strains of approximately 2.5 to 3.0 microstrains. Although this indicates that a larger portion of the load was carried by the box girder on which the load was placed, the lateral load distribution across the segment was nearly uniform. The neutral axis of the box girder is located near the top flange, so the larger magnitudes of strain measured in the bottom flanges could be expected. These figures also show a similar measured strain response between gages whether the test vehicle was positioned in the exterior or interior lanes.

Figures 37 through 40 show measured strain data from the bottom flange gages of segment 62 for the test vehicle located in the southbound traffic lanes. Figures 37 and 38 present strains recorded with the vehicle in the exterior lane, and Figures 39 and 40 show the strains measured with the vehicle in the interior lane. Maximum tensile strains between 2.5 and 3.5 microstrains were recorded by gages 8 and 9 located within the loaded side of the box girder. Gages 17 through 19,

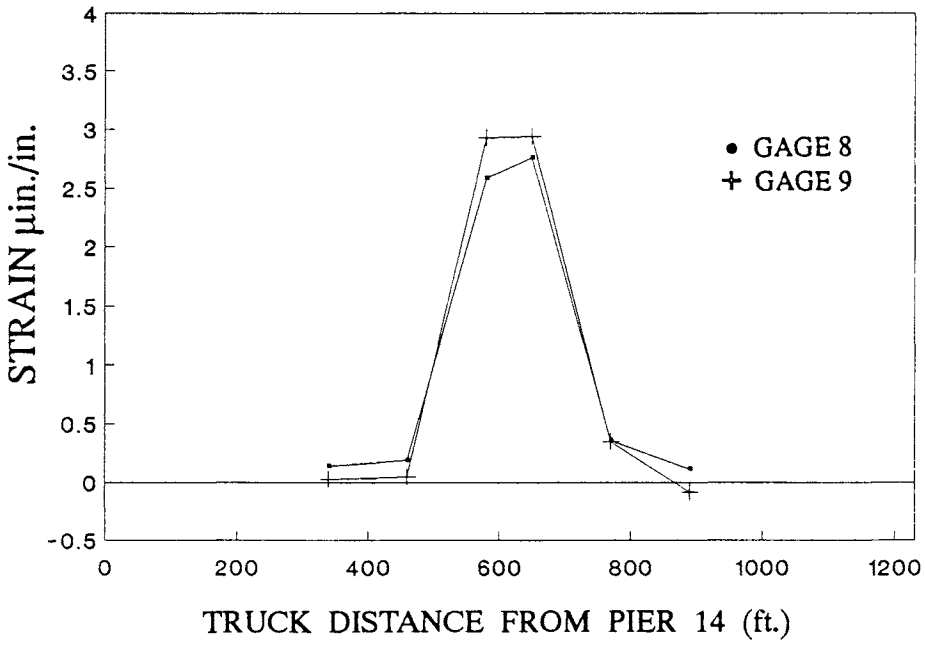

Figure 37. Lower Flange Strains, Segment 62 (Southbound Lane), Vehicle Locations in Southbound Interior Lane.

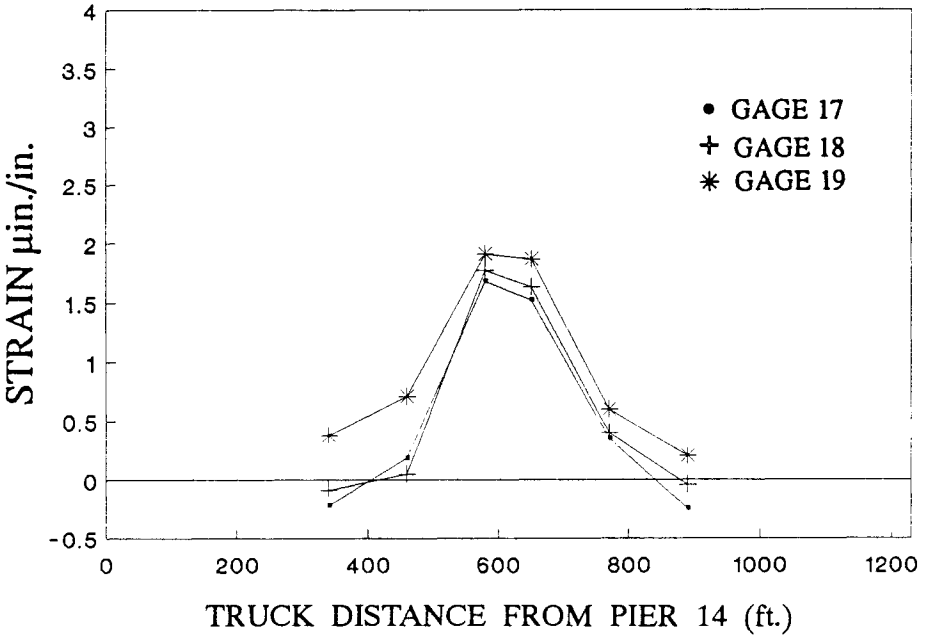

Figure 38. Lower Flange Strains, Segment 62 (Northbound Lane), Vehicle Locations in Southbound Exterior Lane.

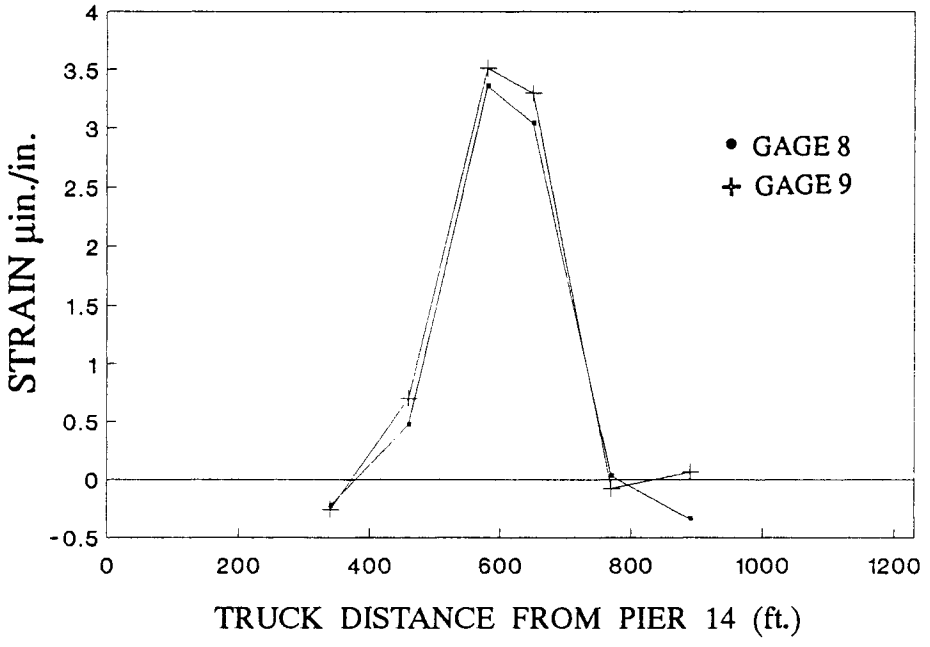

Figure 39. Lower Flange Strains, Segment 62 (Southbound Lane), Vehicle Locations in Southbound Interior Lane.

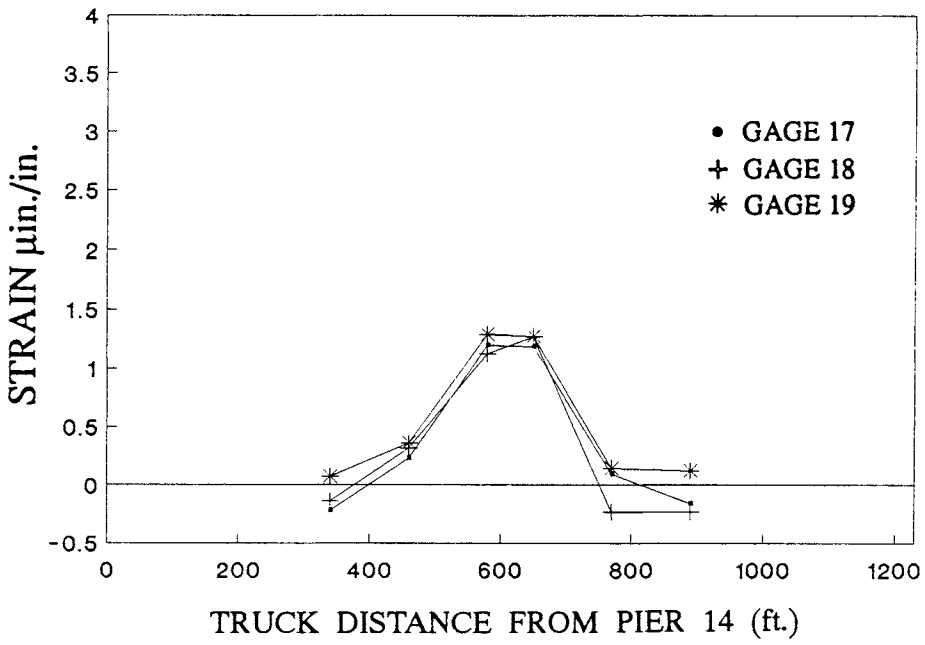

Figure 40. Lower Flange Strains, Segment 62 (Northbound Lane), Vehicle Locations in Southbound Interior Lane.

located in the unloaded portion, indicated maximum strains of approximately 1.0 to 2.0 microstrains. Again, it can be seen that more load was carried by the loaded portion of the twin box girder. Although the variations were more pronounced when the vehicle was located in the southbound lane, the overall difference in transverse load distribution was small. Also, there was little difference between strains measured with the test vehicle in the exterior or interior lanes.

Measured Shear Strain Response

Shear strains were measured in the webs and flanges of the box girder using the three gage strain rosettes described earlier. Because of the previously mentioned malfunctions in the data acquisition system, only two of eight rosettes in segment 33 provided reliable data: rosettes 16 and 18, located respectively in the outside web and bottom flange of the northbound box girder (see Figure 13). Of the four strain rosettes in the webs of box girder segment 62, three yielded reliable data. Again, the strain data obtained from segment 48 are omitted from discussion.

Figures 41 and 42 present the shear strains measured in segment 33 plotted as a function of load position for the test vehicle located in the northbound exterior and interior lanes, respectively. From these figures, it can be seen that small shear strains were observed when the vehicle was in the approach spans and larger strains were measured when it was positioned in the main span, near the instrumented segment. A comparison of Figures 41 and 42 shows that the largest shear strains were recorded in the web directly beneath the load. Smaller magnitudes of

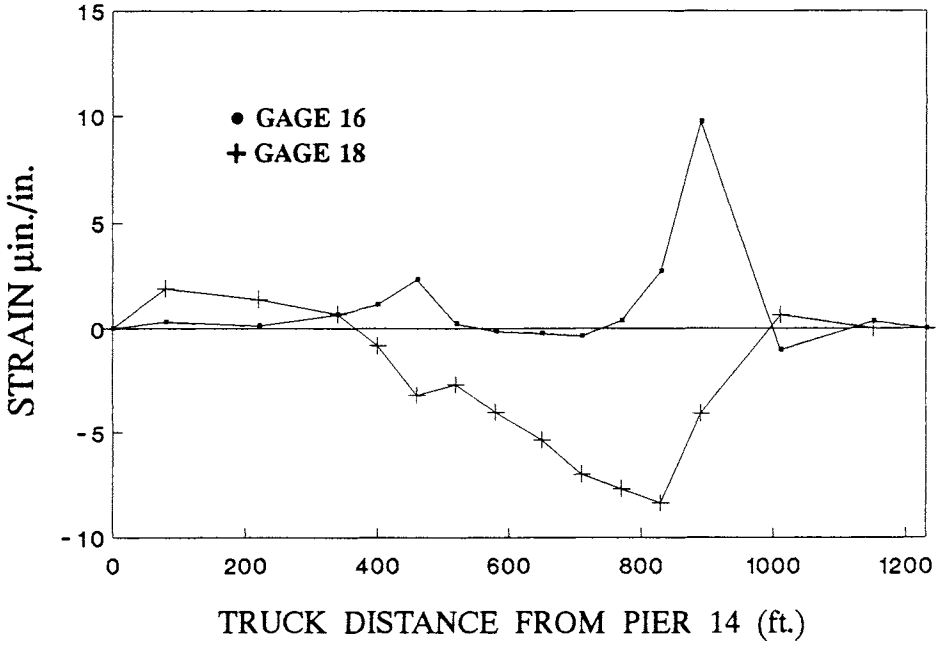

Figure 41. Shear Strains, Segment 33 (Northbound Lane), Vehicle Locations in Northbound Exterior Lane.

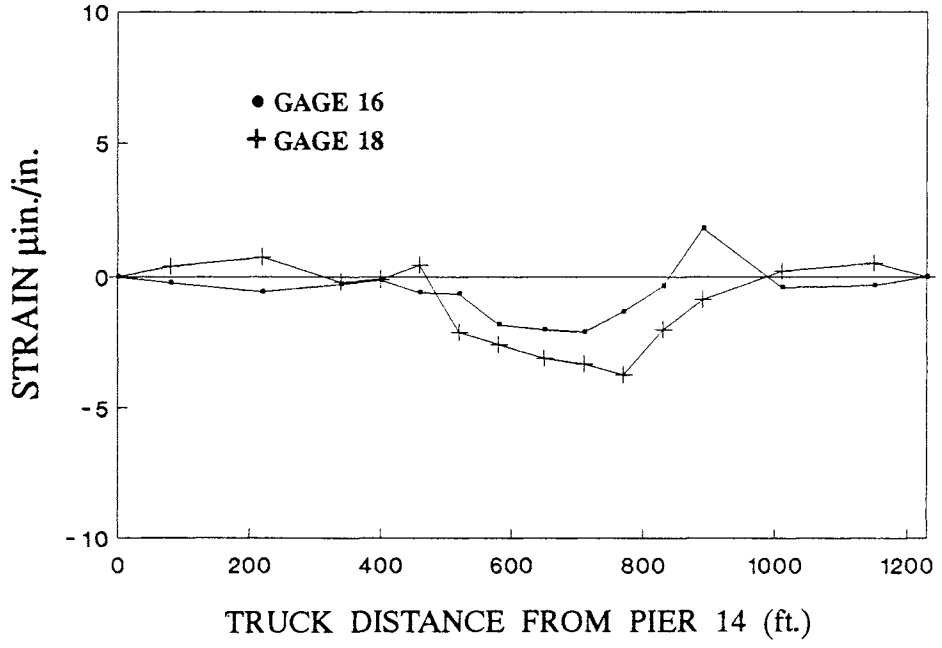

Figure 42. Shear Strains, Segment 33 (Northbound Lane), Vehicle Locations in Northbound Interior Lane.

shearing strain were measured in both the web and flange when the load was in the interior lane.

Shear strains recorded by rosette gages 6, 15, and 16 in the webs of segment 62 are shown in Figures 43 and 44. In these figures, the test vehicle was located in the northbound exterior and interior lanes, respectively. The gages in this segment recorded trends in shear strain response similar to those recorded at segment 33, where larger shear strains occurred as the vehicle neared the midspan segment. An examination of these figures indicates that small shear strains were recorded at gage 6, located in the unloaded portion box girder. With the load in the exterior lane, larger shear strains were measured in the web beneath the load, at gage 16, than in the adjacent web. From Figure 44, it can be seen that the shearing strains were more equally distributed when the test vehicle was located in the interior lane.

The shear strains measured in the webs of segments 33 and 62 show that the individual elements of the box girder cross section behave somewhat independently. With the test vehicle in the exterior lane, higher shear strains were recorded in the outer web of the box girder than at the inner web, suggesting that the loaded web carried more of the shear. Smaller shear strains were measured in the outer web with the vehicle in the interior lane, and the relative magnitudes of strains in the inner and outer webs were about equal. This would indicate that the elements of the box girder section act more as a unit when loaded at these locations, perhaps resulting from the contribution of transverse stiffness from the delta frame assemblies. In addition, the trends in the shear strain response measured at segment 62

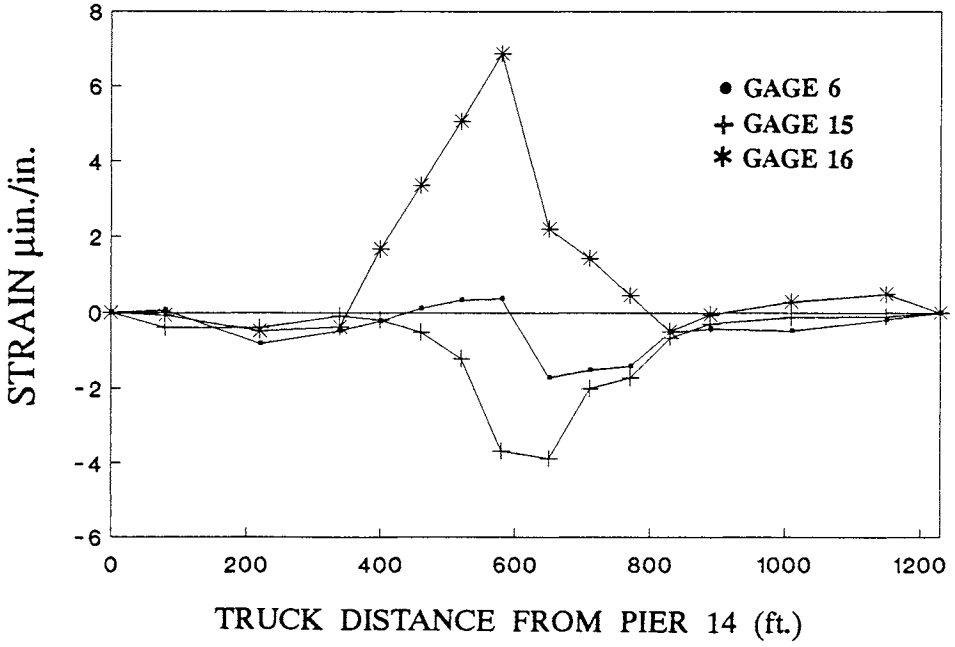

Figure 43. Shear Strains, Segment 62 (Northbound Lane), Vehicle Locations in Northbound Exterior Lane.

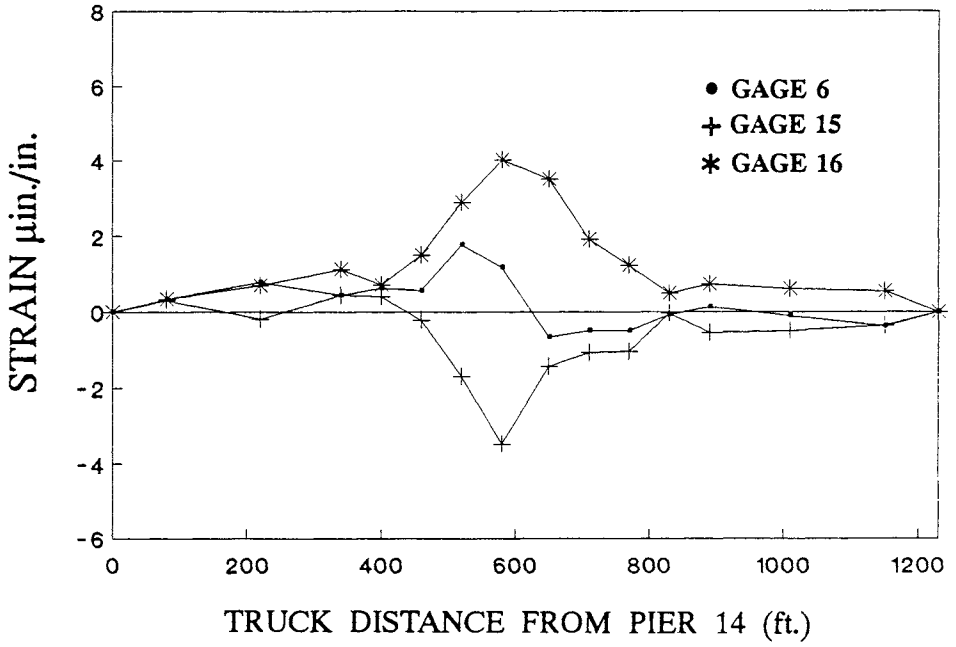

Figure 44. Shear Strains, Segment 62 (Northbound Lane), Vehicle Locations in Northbound Interior Lane.

seem to indicate that the loaded webs carry the shear in bending and the webs away from the load were subject to more torsion. Accurate evaluation of this type of response was somewhat limited because of the small magnitudes of measured shear strain and the combined sensitivity of the rosette gages.

Analytical Studies

Stresses in the top and bottom fibers of the beam elements, corresponding to the top and bottom flanges of the box girder segments, were calculated for all positions of the test load. These stresses are plotted as a function of load position measured from pier 14 in Figures 45 and 46. The magnitudes of the plotted stresses represent the average stress in the top and bottom flanges of box girder segments 33 and 62. For segment 33, the maximum tensile stress in the top flange was calculated to be approximately 8 psi and the maximum compressive stress in the bottom flange was approximately 28 psi. For segment 62, the corresponding stresses were calculated to be approximately 15 and 37 psi, respectively. At the section corresponding to segment 62, it can be seen that essentially zero stresses resulted when the test vehicle was located in the approach spans. Similarly, small stresses were produced at the section corresponding to segment 33 when these spans were loaded.

The variations of strain measured during the field study can be compared with the stress variations predicted by the finite element model, assuming the

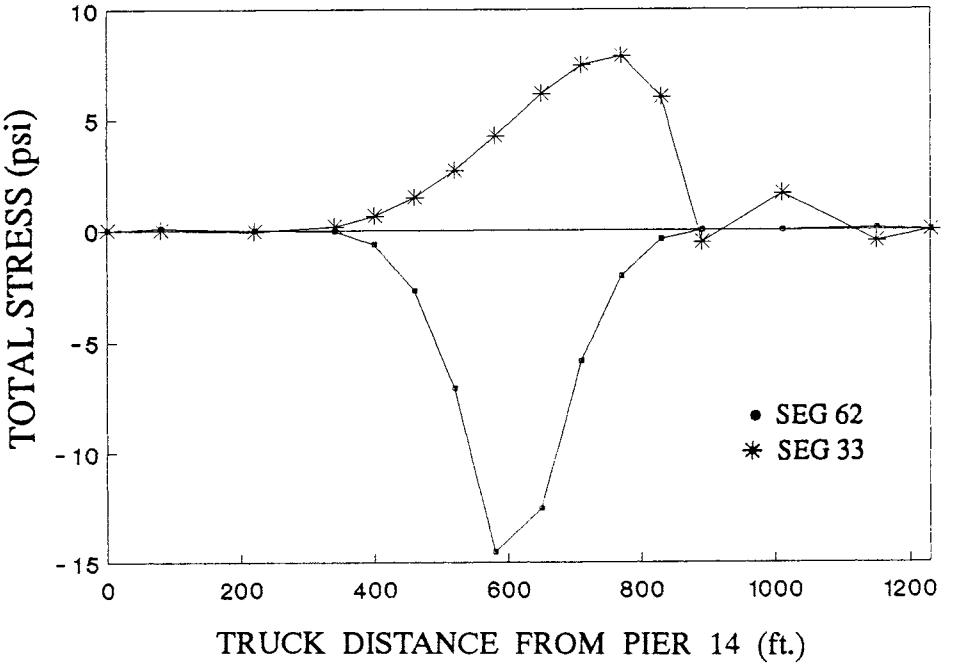

Figure 45. Upper Flange Stresses From Finite Element Model, Segments 33 and 62.

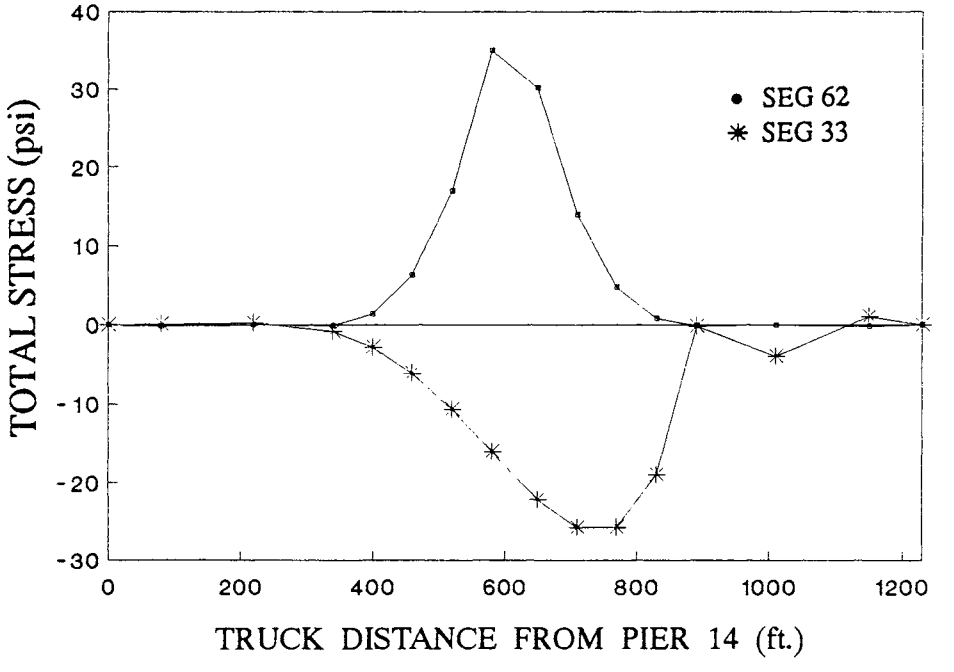

Figure 46. Lower Flange Stresses From Finite Element Model, Segments 33 and 62.

modulus of concrete to be approximately 4.5 million psi. Figures 21 through 23 show the variations in strain in the bottom flange of segment 33, and Figure 46 shows the corresponding values of stress predicted by the finite element model. A comparison of the two figures shows good agreement between the overall trends in strain response. Both measured and predicted stresses were essentially zero until the load entered the main span. The magnitudes of the maximum compressive stresses compare well when the test vehicle was located in the northbound lanes of the box girder. The maximum stresses measured in these cases were approximately 30.0 psi, and maximum stresses between 9.0 and 18.0 psi were measured when the vehicle was positioned in the southbound lanes. The cross-sectional properties of the twin box girder were combined into a single-beam element in the computer model; thus information regarding the transverse distribution of loads was not available.

Stresses in the top flange of the box girder near midspan segment 62 can be compared through examination of the measured data in Figures 29 through 36 and the calculated data in Figure 45. The trends in response from the measured and predicted data show relatively good agreement, though there was some scatter between strain gages. Measured data consistently indicate maximum compressive stresses on the order of 4 to 6 psi, and the corresponding value predicted by the finite element model was approximately 14.5 psi. These measured and predicted values of maximum stress differ by a factor of approximately 3.

Similar comparisons can be made for the bottom flange stresses at segment 62 by examining the measured data in Figures 33 through 40 along with the analytical data in Figure 46. Again, the overall trends in the response were similar in that the tensile stresses peaked as the vehicle approached midspan. Significant differences exist between the magnitudes of the measured and predicted stresses, however. The maximum tensile stress measured in the field test was approximately 12 to 15 psi, and the analytical model yielded a value of 37 psi, as shown in Figure 46. Again, the measured and calculated values of stress response differ by a factor of about 3.

The differences between the measured and predicted stresses warranted a careful review and evaluation of the test procedure and equipment used for measuring strains. The strain data indicated that the heaviest allowable test vehicle produced very small strains in the box girder segments. As a result, calculations of the strain increments attributable to applied vehicle loadings were sensitive to small variations in the zero readings. In certain cases, the temperature changes that occurred during the test caused significant deviations in zero readings. These effects resulted in a relative skew or scattering of the data but were not large enough to cause the large variations in scale between measured and predicted stresses. Otherwise, a source of error in the experimental data could not be found. Likewise, the finite element model appeared to be a reasonable representation of the bridge and provided accurate estimates of natural frequencies in dynamic analyses (Lissenden, 1988).

DISCUSSION

The applied test loading was of relatively small magnitude compared to the self-weight of the bridge. The weight of the vehicle was approximately 50,000 lb, and the weight of each of the 124 single box girder segments was roughly 135,000 lb. The strains and corresponding stresses produced by this loading were small in absolute magnitude. For example, the largest strain values recorded during the load test were on the order of 5 to 10 microinches per inch (microstrains), associated with changes in stress of approximately 20 to 50 psi. Although small, the reliability of the recorded strain values was substantiated by the fact that the readings were reproduced with little error under repeated load applications and recorded values of strain were consistent between gages at different locations within the instrumented segments.

The study indicated that reliable experimental strain data could be measured when the applied load was only approximately 0.5 percent of the weight of the bridge superstructure. When plotted as a function of load position, the measured strain data varied in a manner generally consistent with expected response. Corresponding variations in stress were in general agreement with those predicted by the computer model; however, the magnitudes of these stresses differed considerably at the midspan of the bridge.

Evaluations of the experimental procedure and analytical model did not yield an explanation for the differences between the magnitudes of the measured and calculated stresses. If both the measured and predicted responses are to be accepted, it would suggest the possibility that some aspect of the actual structure is not adequately represented in the finite element model. This may indicate, for example, that some unrecognized patterns of load transfer may be taking place within the structure or that complete continuity might not exist at midspan. In the latter case, the post-tensioning and closure pour joining the two cantilever sections of the main span may have resulted in less than full continuity within the span, which could lead to lower stresses at midspan.

Though some differences exist between the measured and predicted response, both clearly illustrate the high degree of stiffness and load-carrying capacity of the bridge. Both the measured and predicted maximum stresses resulting from a single truck loaded to legal limits were well under 50 psi. This field test points out the fact that, although finite element models can be useful analysis tools for predicting the behavior of complex structures, considerable care should be taken that these models accurately represent the actual structure. Continued field testing of structures such as cable-stayed bridges is an essential element in achieving this end.

This study revealed the many difficulties associated with field instrumentation and testing of structures, especially under construction conditions. The individual bridge segments were formed in the casting yard at the foot of the bridge. Although it was easier to install the instrumentation here, rather than on the structure itself, there were logistical problems with materials and scheduling, which were further compounded by the 90-mile driving distance between the bridge and

VTRC. Despite the best efforts of the researchers, it was difficult to protect the equipment from damage caused by construction activities. As a result, a significant number of strain gages were inoperative and constant repairs to the data lines were necessary. Also, the harsh construction and field environment was damaging to the sensitive electronic equipment and has led to serious questions concerning the reliability of the data acquisition system.

Analysis of the measured strain data indicated a number of deficiencies in the instrumentation and data acquisition system. Malfunctions within the remote scanning chasses were difficult to diagnose and repair and resulted in significant losses of data.

Although the measured data were determined to represent the actual response of the structure, a critical evaluation of each component of the strain measuring instrumentation raised serious questions regarding the reliability of the data acquisition system. Installation of another system of strain measuring devices, such as Carlson strain meters, in addition to the strain-gaged rebar, would provide an independent check on the system components. The small magnitudes of strain measured were near the sensitivity limit of the gages themselves. Loading the bridge with more than one truck would have resulted in larger strains, thereby allowing for improved evaluation of measured strain response.

CONCLUSIONS

1. The experimental strains measured in the I-295 bridge showed the same trends as those obtained from finite element models. Quantitative agreement between measured and computed strains was fairly good for segment 33 but poor at segment 62. This may be attributable in part to the relatively small magnitude of live load that could be applied relative to the bridge dead load. It cannot be ruled out, however, that the bridge continuity conditions were somewhat different than those assumed in the finite element model, particularly at midspan.

2. The shear strains computed from the field measurements tended to indicate that the shear strain over a loaded web was dominated by bending, but the shear strain in the webs not loaded was dominated by torsions. This suggests that significant local distortion of the twin box girder system was present, even with the stiffening delta frames.

3. Load tests on complex bridge structures, such as the I-295 bridge, have the potential to reveal differences between actual field behavior and computational idealizations. This can lead to improved computational models and a better understanding of the as-constructed state of structures. If this potential is to be fully realized, very carefully designed instrumentation chosen with this objective in mind is necessary.

4. The strain gages appeared to be sensitive to thermal strains. Even though a baseline correction was used to minimize this influence, it was not possible to

eliminate it. These effects are discussed more fully by Duemmel et al. (1992) and include the influence of curvature in the mounted transverse strain gages and mechanical strain caused by mismatch in the coefficients of thermal expansion of the bridge concrete and steel.

5. Malfunctioning of the data acquisition system appeared to invalidate some of the data. Although considerable time was spent attempting to troubleshoot and repair the system, it was not possible to eliminate the problem.

RECOMMENDATIONS

1. A variety of computational/analytical models have been developed for analysis of box girder bridges. A comprehensive comparison of these methods does not appear to be available at this time. As box girder bridges promise to be widely used in years to come, consideration of the relative efficiency and accuracy of these methods appears to be warranted.

2. A review of the current literature showed that many developments have been made in the analysis of box girder bridges. More information from field measurements of actual bridge response is needed for verification of range of analytical or computational models that can now be constructed.

3. Strain gage systems for field instrumentation of reinforced or prestressed concrete structures must function adequately under much more demanding conditions than laboratory-mounted systems. Specifically, it appears that, rather than eliminate thermal strain measurements, it may be preferable to record them, together with the actual temperature changes at each gage. Thus, such actual physical phenomena as coefficient of thermal expansion mismatches may be considered. Further consideration of the most appropriate strain gage systems to use for instrumentation of cast-in-place and precast concrete structures under field conditions appears warranted.

REFERENCES

Baber, T.T., & Hilton, M.H. (1988). *Field monitoring on the I-295 bridge over the James River: Instrumentation installation and construction period studies.* Charlottesville: Virginia Transportation Research Council.

Barton, F.W., Baber, T.T., Ramsey, R.D., & McKeel, W.T., Jr. (1990). Measured stresses in the deck segments of a cable-stayed bridge. *Proceedings of the ASCE Structures Congress.* New York: ASCE.

Barton, F.W., Baber, T.T., Duemmel, P.S., & McKeel, W.T., Jr. (1991). Field test of a cable-stayed bridge. *Transportation Research Record 1290.* Washington, DC: Transportation Research Board.

Batla, F.A., Reisnour, P.R., & Pathak, D.V. (1984). Finite element program for analysis of folded plate bridge superstructures. *Transportation Research Record 950.* Washington, DC: Transportation Research Board.

Boswell, L.F., & Zhang, S.H. (1984). The effect of distortion in thin-walled box-spine beams. *International Journal of Solids and Structures,* 20: 845-862.

Chang, S.T., & Zheng, F.Z. (1987). Negative shear lag in cantilever box girders with constant depth. *Journal of Structural Engineering,* 113(1): 20-35.

Cheung, M.S., & Wenchang, L. (1989). Analysis of continuous, haunched box girder bridges by finite strips. *Journal of Structural Engineering*, 115(5): 1076-1087.

Choudhury, D., & Scordelis, A.C. (1988). Structural analysis and response of curved prestressed concrete box girder bridges. *Transportation Research Record 1180.* Washington, DC: Transportation Research Board.

Duemmel, P.S., Baber, T.T., Barton, F.W., & McKeel, W.T., Jr. (1992). *Field instrumentation and measured response of the I-295 cable-stayed bridge: Part 2—Field study of thermal responses.* VTRC Report No. 92-R21, Charlottesville: Virginia Transportation Research Council.

Evans, H.R., & Rowlands, D.V. (1985). An experimental and theoretical investigation of the behavior of box girders on skew supports. *Civil Engineering for Practicing and Design Engineers*, 4(3): 211-230.

Floyd, D.W., & Sutton, C.D. (1982). *Study of the segmental box girder bridge at Turkey Run: Summary report.* Joint Highway Research Project Report JHRP-82/16. West Lafayette: Purdue University/Indiana State Highway Commission.

Foutch, D.A., & Chang, P.C. (1982). A shear lag anomaly. *Journal of Structural Engineering,* 108(7): 1653-1658.

Hayes, S.W. (1988). *Implementation of the data acquisition system for the I-295 James River Bridge.* Masters thesis. Charlottesville: University of Virginia, Department of Civil Engineering.

Ishac, I.I., & Graves Smith, T.R. (1985). Approximations for moments in box girders. *Journal of Structural Engineering*, 111(11): 2333-2342.

Kanok-Nukulchai, W., & Sivakumar, M. (1988). Degenerate elements for combined flexural and torsional analysis of thin-walled structures. *Journal of Structural Engineering*, 114(3): 657-674.

Kristek, V., & Bazant, Z.P. (1987). Shear lag effect and uncertainty in concrete box girder creep. *Journal of Structural Engineering*, 113(3): 557-574.

Kristek, V., & Evans, H.R. (1985). A hand calculation of the shear lag effect in unstiffened flanges and in flanges with closely spaced stiffeners. *Civil Engineering for Practicing and Design Engineers*, 4(2): 163-190.

Kristek, V., & Studnicka, J. (1988). Negative shear lag in cantilever box girders with constant depth: Discussion. *Journal of Structural Engineering*, 114(9): 2168-2172.

Kuzmanovic, B.O., & Graham, J. (1981). Shear lag in box girders. *Journal of Structural Engineering*, 107(9): 1701-1712.

Kuzmanovic, B.O., & Sanchez, M.R. (1986). Lateral distribution of live loads on highway bridges. *Journal of Structural Engineering*, 112(8): 1847-1862.

Li, W.Y., Tham, L.G., & Cheung, Y.K. (1988). Curved box girder bridges. *Journal of Structural Engineering*, 114(6): 1324-1338.

Lissenden, C.J. (1988). *Dynamic modelling of a cable-stayed bridge during construction*. Masters thesis. Charlottesville: University of Virginia, Department of Civil Engineering.

Loo, Y.C., & Srivanich, S. (1983). A simplified analysis of cable-stayed box bridges. *International Journal of Structures*, 3(3): 93-103.

Maisel, B.I. (1982). *Analysis of concrete box beams using small computer capacity.* Development Report 5. London: Cement and Concrete Association.

Maisel, B.I. (1986). Shear lag analysis of concrete box beams using small computer capacity. *Proceedings of the Second Canadian Society of Civil Engineers: International Conference on Short and Medium Span Bridges*, Vol. 1, pp. 125-137. Ottawa, Ontario, Canada: Canadian Society of Civil Engineers.

Maisel, B.I., & Roll, F. (1974). *Methods of analysis and design of concrete box beams with side cantilevers*. Technical Report 42.494. London: Cement and Concrete Association.

Mathivat, J. (1983). *The cantilever construction of prestressed concrete bridges.* New York: John Wiley & Sons.

Mavaddat, S., & Mirza, M.S. (1989). Computer analysis of thin walled concrete box beams. *Canadian Journal of Civil Engineering,* 16(6): 902-909.

Measurements Group, Inc. (1983). *Temperature induced apparent strain and gage factor variation in strain gages.* Measurements Group Technical Note No. TN-504. Raleigh, NC.

Mikkola, M.J., & Paavola, J. (1980). Finite element analysis of box girders. *Journal of Structural Engineering,* 106(6): 1342-1357.

Mohr, M. (1989). *The strain gage instrumentation of cables on the I-295 James River cable-stayed bridge.* Masters thesis. Charlottesville: University of Virginia, Department of Civil Engineering.

Muller, J.M., & McCallister, L.F. (1988). Esthetics and concrete segmental bridges in the United States. *Concrete International*, 10(5): 25-33.

Murtuza, M.A., & Cope, R.J. (1985). Investigation of concrete spine beam bridge decks. *Journal of the American Concrete Institute*, 82(2): 162-169.

Nam Shiu, K. (1985). *Instrumentation of the Red River Bridge at Boyce, Louisiana: Interim Report No. 1.* Skokie, IL: Portland Cement Association, Construction Technology Laboratories.

Nam Shiu, K., Daniel, J.I., & Russell, H.G. (1983). *Time dependent behavior of segmental cantilever concrete bridges.* Report to the State of Illinois, Department of Transportation. Skokie, IL: Portland Cement Association, Construction Technology Laboratories.

Podolny, W., Jr. (1985). The causes of cracking in post-tensioned concrete box girder bridges and retrofit procedures. *Prestressed Concrete Institute Journal,* March/April, pp. 82-139.

Podolny, W., Jr. (1986). Evaluation of transverse flange forces induced by laterally inclined longitudinal post-tensioning in box girder bridges. *Prestressed Concrete Institute Journal*, January/February, pp. 44-61.

Razaqpur, A.G., & Li, H.G. (1990). Analysis of multi-branch multi-cell box girder bridges. *Proceedings of the Developments in Short and Medium Span Bridge Engineering '90*, Vol. 1, pp. 153-164. Toronto, Ontario, Canada: Canadian Society of Civil Engineers.

Russell, H.G., Nam Shiu, K., Gamble, W.L., & Marshall, V.L. (1982). Evaluation and verification of time dependent deformations in posttensioned box girder bridges. *Transportation Research Record 871.* Washington, DC: Transportation Research Board.

Scordelis, A.C., Watsi, S.T., & Seible, F. (1982a). Structural response of skew RC box girder bridge. *Journal of Structural Engineering*, 108(1): 89-104.

Scordelis, A.C., Watsi, S.T., & Seible, F. (1982b). Ultimate strength of skew RC box girder bridge. *Journal of Structural Engineering*, 108(1): 105-121.

Shushkewich, K.W. (1986). Membrane forces acting on a box girder bridge. *Journal of Structural Engineering*, 112(8): 1900-1907.

Shushkewich, K.W. (1988). Approximate analysis of concrete box girder bridges. *Journal of Structural Engineering*, 114(7): 1644-1657.

Song, Q., & Scordelis, A.C. (1990a). Shear lag analysis of T-, I-, and box beams. *Journal of Structural Engineering*, 115(5): 1290-1305.

Song, Q., & Scordelis, A.C. (1990b). Formulas for shear lag effect in T-, I-, and box beams. *Journal of Structural Engineering,* 115(5): 1306-1318.

Vlasov, V.Z. (1961). *Thin-walled elastic beams.* Jerusalem: Israel Program for Scientific Translations.

Waldron, P. (1986). Stiffness analysis of thin-walled girders. *Journal of Structural Engineering*, 112(6): 1366-1384.

Waldron, P., Ramezankhani, M., & Woodman, N. (1990). Differential temperature effects in concrete box girder bridges. *Proceedings of the Developments in Short and Medium Span Bridge Engineering '90*, Supplement, pp. 1-12. Toronto, Ontario, Canada: Canadian Society of Civil Engineers.

Zhang S.H., & Lyons, L.P.R. (1984). A thin-walled box beam finite element for curved bridge analysis. *Computers and Structures*, 18(6): 1035-1046.